European Journal of Medicinal Chemistry 259 (2023) 115663

Contents lists available at ScienceDirect

European Journal of Medicinal Chemistry

journal homepage: www.elsevier.com/locate/ejmech

Research paper

Targeted theranostics: Near-infrared triterpenoic acid-rhodamine conjugates as prerequisites for precise cancer diagnosis and therapy

Niels Heise [a], Florian Lehmann [b], René Csuk [a,*], Thomas Mueller [c]

[a] Martin-Luther-University Halle-Wittenberg, Organic Chemistry, Kurt-Mothes-Str. 2, D-06120, Halle (Saale), Germany
[b] Martin-Luther-University Halle-Wittenberg, Physical Chemistry, von-Dankelmann-Platz 4, D-06120, Halle (Saale), Germany
[c] Martin-Luther-University Halle-Wittenberg, Medical Faculty, University Clinic for Internal Medicine IV, Hematology/Oncology, Ernst-Grube-Str. 40, D-06120, Halle (Saale), Germany

ARTICLE INFO

Keywords:
Asiatic acid
Cytotoxicity
Changsha dye
NIR-Fluorescence
Theranostics

ABSTRACT

Pentacyclic triterpenoic acids have shown excellent potential as starting materials for the synthesis of highly cytotoxic agents with significantly reduced toxicity for non-malignant cells. This study focuses on the development of triterpenoic acid-rhodamine conjugates with fluorescence shifted to the near-infrared (NIR) region for theranostic applications in cancer research. Spectral analysis revealed emission wavelengths around $\lambda = 760$ nm, enabling stronger signals and deeper tissue penetration. The conjugates were evaluated using SRB assays on tumor cell lines and non-malignant fibroblasts, demonstrating low nanomolar activity and high selectivity, similarly to their known rhodamine B counterparts. Additional staining experiments proved their mode of action as mitocans.

1. Introduction

Cancer is a major public health concern, and despite significant advances in cancer research and treatment, cancer remains a leading cause of death. [1] Diagnosis and treatment, or the course of treatment and the decision to continue or stop treatment, are usually carried out using different methods and at different times. In recent years, theranostics has emerged as a promising approach for the simultaneous identification and treatment of cancer. [2,3] This has several advantages: First, theranostics allows targeted therapies directly to cancer cells while sparing healthy tissue. Thereby the risk of side effects associated with traditional treatments is avoided or minimized. Second, theranostics allows to create personalized treatment plans for individual patients, hence improving the overall efficacy of the treatments, and finally, theranostics enables to monitor the effectiveness of treatment in more-or-less real-time; this fact ensures most effective treatments while again minimizing the risk of side effects.

Pentacyclic triterpenoic acids have been shown to be excellent starting materials for the synthesis of highly cytotoxic agents while being significantly less cytotoxic for non-malignant tissue. Thereby conjugates consisting of a di- or tri-acetylated triterpene, a suitable amide spacer at the distal position of the triterpene and a rhodamine proved to be especially promising molecules. [4–11] For example, an asiatic acid derived conjugate (**AAHR**, Fig. 1) held cytotoxic activity in sub-nanomolar concentration, and was also able to be effective even in multiple resistant cell lines, was active in 3D spheroids and acted as a mitocan by shutting down mitochondrial ATP production. [12].

Despite their superior cytotoxicity, these compounds, however, proved unsuitable for *in vivo* studies because their absorption and emission wavelengths were limited to the ultraviolet and visible regions. In recent years, near-infrared (NIR) fluorescence imaging has emerged as a powerful tool for *in vivo* imaging of biological processes and molecular events in living cells and tissues, including tumor growth and response to therapy. [13–16] By incorporating fluorescent tags, bio-distribution and efficacy can be monitored *in vivo* in real time, allowing rapid optimization of their structure and dosing regimen. They offer deeper tissue penetration, reduced background fluorescence and improved signal-to-noise ratio. However, the development of efficient NIR fluorescent probes remains challenging due to the lack of suitable fluorophores and design strategies. [17,18] Hereby, we report the development of a new class of triterpenoic acid-rhodamine conjugates with fluorescence shifted to the NIR region. This has been achieved by redesigning the fluorophore so that it retains its photo-physical properties but emits in the NIR when excited by higher wavelength light sources but it also keeps its cytotoxic properties. Fluorescence wavelengths are highly dependent on the substituents attached to the amino

* Corresponding author.
E-mail address: rene.csuk@chemie.uni-halle.de (R. Csuk).

https://doi.org/10.1016/j.ejmech.2023.115663
Received 21 June 2023; Received in revised form 12 July 2023; Accepted 16 July 2023
Available online 17 July 2023

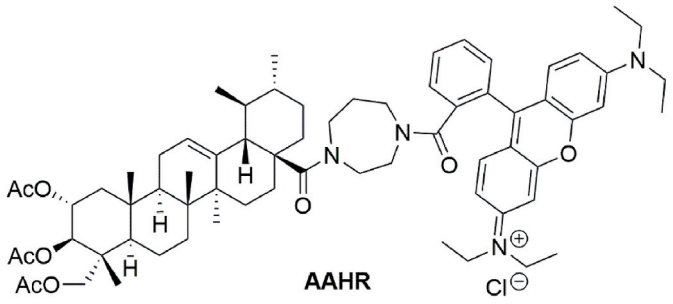

Fig. 1. Structure of mitocanic homopiperacinyl linked asiatic acid rhodamine B conjugate **AAHR** of superior cytotoxic activity.

group of the rhodamine. [19] Quite recently, a new type of NIR functional dyes has been introduced, i.e., the Changsha (CS) NIR dyes. These dyes are hybrids of a merocyanine and a benzoic acid derivative. [20] Due to its high structural similarity to rhodamine B (calculated maximum common substructure MCS = 0.72), we decided that the dye CS-2 (Fig. 2) should be suited to label triterpenoic acids thus allowing us to investigate whether these hybrids would be able to act as cytotoxic agents (preferentially as a mitocan) and to work as a probe for malignant cells.

Changsha-type dyes have previously been used for biological imaging of HClO in living mice [21], to measure lysosomal pH inside endothelial and breast cancer cells [22], to image glutathione in HepG2 cells [23–25], and as a chemo-dosimeter for Mg^{2+}, Al^{3+} and Cu^{2+} ions but also for some markers of hepatotoxicity [26–28]. Recently a glycyrrhetinic acid decorated conjugate was shown to be taken up in lysosomes of liver cancer cell lines HepG2 and Huh7 thereby allowing imaging of hepatocellular carcinoma. [29].

2. Results and discussion

The synthesis of CS-2 (**1**) was accomplished according to literature. [20] Thus, condensation of a commercially available substituted benzoic acid (**A**, Scheme 1) with cyclohexanone (**B**) under acidic conditions followed by reaction with the corresponding Fisher base **C** in acetic anhydride afforded the substituted CS-2 rhodamine **1** as a dark green solid in 50% overall yield.

Acetylation of triterpenoic acids, oleanolic acid (**OA**, Scheme 2), ursolic acid (**UA**), corosolic acid (**CA**) and asiatic acid (**AA**) gave the known acetates **2**, **7**, **12**, and **17**, respectively. Their carboxyl group was activated with oxalyl chloride followed by the addition of either piperazine or homopiperazine to afford the corresponding amides **3**, **4**, **8**, **9**, **13**, **14**, **18** and **19**. Activation of the CS-2 rhodamine **1** with oxalyl chloride and its reaction with the amine-spaced triterpenoic acids yielded the desired conjugates **5**, **6**, **10**, **11**, **15**, **16**, **20** and **21**, respectively.

To demonstrate their suitability for NIR experiments, fluorescence spectra were recorded and compared with those of conjugates derived from rhodamine B. Thereby, the samples were irradiated at a fixed excitation wavelength of λ = 580 nm or λ = 430 nm to obtain the emission spectra (Fig. 3) The wavelength of maximum fluorescence intensity was used as the fixed emission wavelength to obtain the excitation spectrum of each compound (Fig. 4).

Comparing the maximum excitation wavelength of the rhodamine B and CS-2 (**1**) as well as of conjugates **AAHR** and CS-2 conjugate **21** a shift of maximum excitation wavelengths to higher wavelengths can be observed for **1** and compound **21** as compared to the corresponding rhodamine B analogs (Fig. 4). This is particularly important for applications such as fluorescence-guided surgery and imaging of deep-seated tumor cells inasmuch as less photo-damaging in biological samples can be expected. In addition, biological probes excited by higher wavelength light sources often exhibit less background fluorescence, resulting in an improved signal-to-noise ratio and better image quality. These observations are based on the fact that many biological samples such as tissues and cells, naturally fluoresce at lower wavelengths, which can interfere with the detection of fluorescent probes excited at UV wavelengths.

The wavelength of the emitted light has been shifted from around λ = 590 nm in rhodamine B conjugates to λ = 760 nm for the CS-2 conjugates (Fig. 5).

As a result, the latter conjugates should be able to generate stronger signals from deeper tissue depths, making them extremely valuable for detecting and monitoring biological processes deep inside living organisms using highly sensitive imaging systems such as high-resolution microscopes and endoscopic imaging devices.

The CS-2 conjugates **5**, **6**, **10**, **11**, **15**, **16**, **20**, **21** were analyzed using SRB cytotoxicity assays, thereby using a selection of human tumor cell lines representing different solid tumor entities and non-malignant human fibroblasts (CCD18Co) to assess both their anti-proliferative/cytotoxic activity and their tumor cell/non-tumor cell selectivity. In addition, our panel included the cell line pair A2780/A2780cis, a well-known model of acquired drug resistance to conventional drugs such as cisplatin and doxorubicin. The results from these assays are summarized in Table 1 and in Figs. 6 and 7.

As a result, a compound and cell line dependent cytotoxic activity in the nanomolar range could be established (see Fig. 8). In general, conjugates from asiatic acid were more cytotoxic than their analogs derived from corosolic, oleanolic and ursolic acid, thereby resulting in single to three-digit nanomolar IC_{50} values. In each case, the homopiperazinyl linker led to an increased cytotoxic activity independently of the type of triterpene carboxylic acid. Furthermore, the A2780 cell line was the most sensitive model compared to the least sensitive model MCF7, with up to 12-fold differences in their IC_{50} values. The most active compounds (**16**, **20**, **21**) were also the most selective, as assessed by two different selectivity indices based on the most and least sensitive cell lines. The relative resistance of A2780cis compared to A2780 was reproduced in additional assays using doxorubicin, resulting in an approximately 10-fold difference in their IC_{50} values. The compounds were able to reduce this resistance by up to 5-fold. The analysis of subcellular localization for the CS2-hybrides proved the expected mitochondrial targeting. Thereby compounds **16**, **20** and **21** mostly

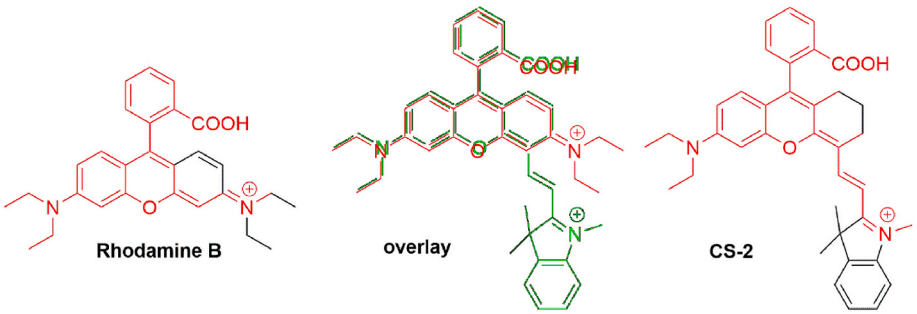

Fig. 2. Comparison of rhodamine B and CS-2 (**1**).

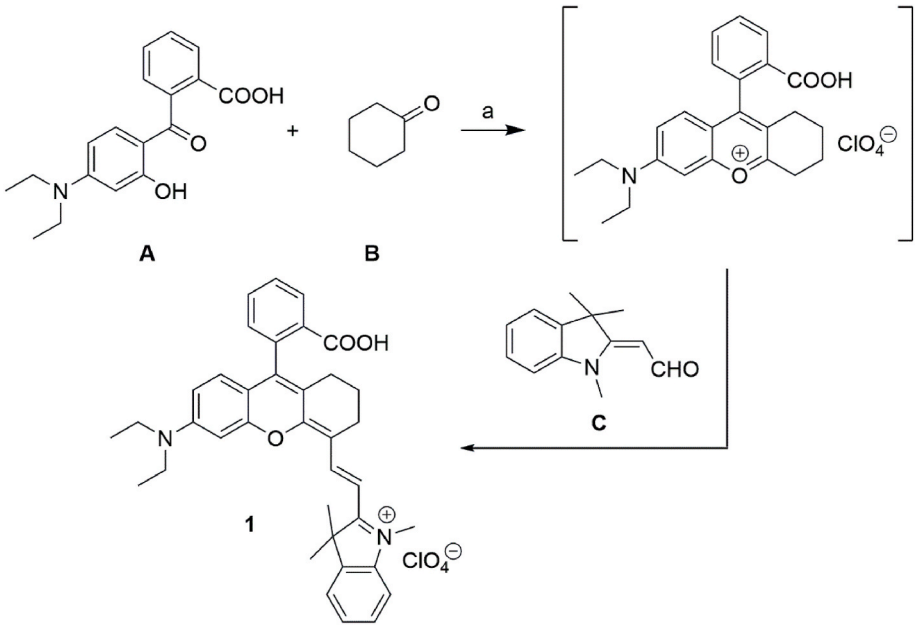

Scheme 1. Synthesis of the Changsha dye CS-2 **1**. Reactions and conditions: a) conc. H_2SO_4, 90 °C, 90 min; then $HClO_4$; b) Ac_2O, 50 °C; over-all yield: 50%.

resemble the accumulation pattern of BioTracker 488 and well known **AAHR**, whereas those derivatives holding less acetoxy groups showed a different pattern and also seem to accumulate partially in the nucleus. In addition, the subcellular localization of the most active compounds **20** and **21** was further investigated performing co-treatment of compounds together with BioTracker 488 and Hoechst 33342 (nucleus) enabling simultaneous analysis of localization. Furthermore, multiple Z-stacked images at a higher magnification were taken allowing a more precise reconstruction of localization. This analysis confirmed the mitochondria as the main target of compound **20** and **21** (Fig. 9).

3. Conclusion

Our studies confirm the initial hypothesis that not only the triterpene backbone and the type of amide, but also the number of acetoxy groups and the linkage position of the rhodamine residue significantly influence the cytotoxic activity and tumor cell selectivity. Furthermore, the best performing compound **21** showed very similar characteristics in terms of cytotoxicity and selectivity as well as subcellular accumulation pattern compared to the chemical/structural congener containing the rhodamine B residue (**AAHR**) reported in our previous study. Thus, the specific modification of the rhodamine to obtain near-infrared spectral properties does not affect the efficacy of the compounds and proves these compounds as useful probes for further biological evaluation.

4. Experimental part

4.1. General

Fluorescence spectra were recorded using an Edinburgh Instruments FS5 spectrofluorometer. The measured methanolic dye solutions were placed in a 10 mm quartz cuvette with a filling volume of 500 μL. The samples were irradiated with a 150 W CW ozone-free xenon lamp at room temperature. The emitted photons were counted in 1 nm steps for 0.5 s. To record the spectra of CS-2 rhodamine solutions, the width of the excitation and emission light paths was set to 3 mm and 2.5 mm respectively. The samples were irradiated at a fixed excitation wavelength of $\lambda = 580$ nm to obtain the emission spectra. The wavelength of maximum fluorescence intensity was used as the fixed emission wavelength to obtain the excitation spectrum of each individual CS-2 rhodamine dye. To obtain the spectra of the modified rhodamine B solutions, the width of the excitation and emission light paths was reduced to 1 mm due to the very high intensity of the fluorescent light. The samples were irradiated at a fixed excitation wavelength of $\lambda = 430$ nm to obtain the emission spectra. The wavelength of maximum fluorescence intensity was used as the fixed emission wavelength to obtain the excitation spectrum of each individual rhodamine B dye.

TLC was carried out on silica gel (Macherey-Nagel, detection under UV light and with cerium molybdate reagent). The used solvents were dried according to usual procedures. Melting points are uncorrected (Leica hot stage microscope, or BÜCHI melting point M – 565). IR spectra were recorded on a PerkinElmer FT-IR spectrometer Spectrum 1000 or on a Perkin-Elmer Spectrum Two (UATR Two Unit). Optical rotations were measured using a JASCO-2000P instrument; no values can be provided for the deeply colored solutions of the Changsha conjugates. NMR spectra were recorded using the Agilent spectrometers DD2 500 MHz and VNMRS 400 MHz (δ given in ppm, J in Hz; typical experiments: APT, H–H–COSY, HMBC, HSQC, NOESY), MS spectra were taken on an Advion Expression CMS instrument, and elemental analyses were conducted on a Foss-Heraeus Vario EL (CHNS) unit. Rhodamine B as well as the triterpenoic acids were obtained from local vendors and used as received. The SRB assays were performed as previously reported.

4.2. Cell culture

The human cancer cell lines A2780 (ECACC #93112519), A2780Cis (ECACC # 93112517), A549 (ATCC - CCL-185), HT29 (ATCC - HTB-38), MCF7 (ATCC - HTB-22) were cultivated in RPMI1640 medium, non-malignant human fibroblasts CCD18Co (ATCC - CRL-1459) were grown in MEME (both from Sigma-Aldrich, St. Louis, MO, USA). Both media were supplemented with 10% fetal bovine serum (Biowest, Nuaillé, France) and 1% penicillin-streptomycin (Sigma-Aldrich).

4.3. SRB assay

Cytotoxic activities of compounds were analyzed using the SRB cytotoxicity assay. Cells were seeded in 96-well plates and after 24h were treated with serial dilutions of compounds for 72 h. All subsequent steps were performed according to the previously described SRB assay protocol. [30] Dose-response curves and calculation of IC_{50} values

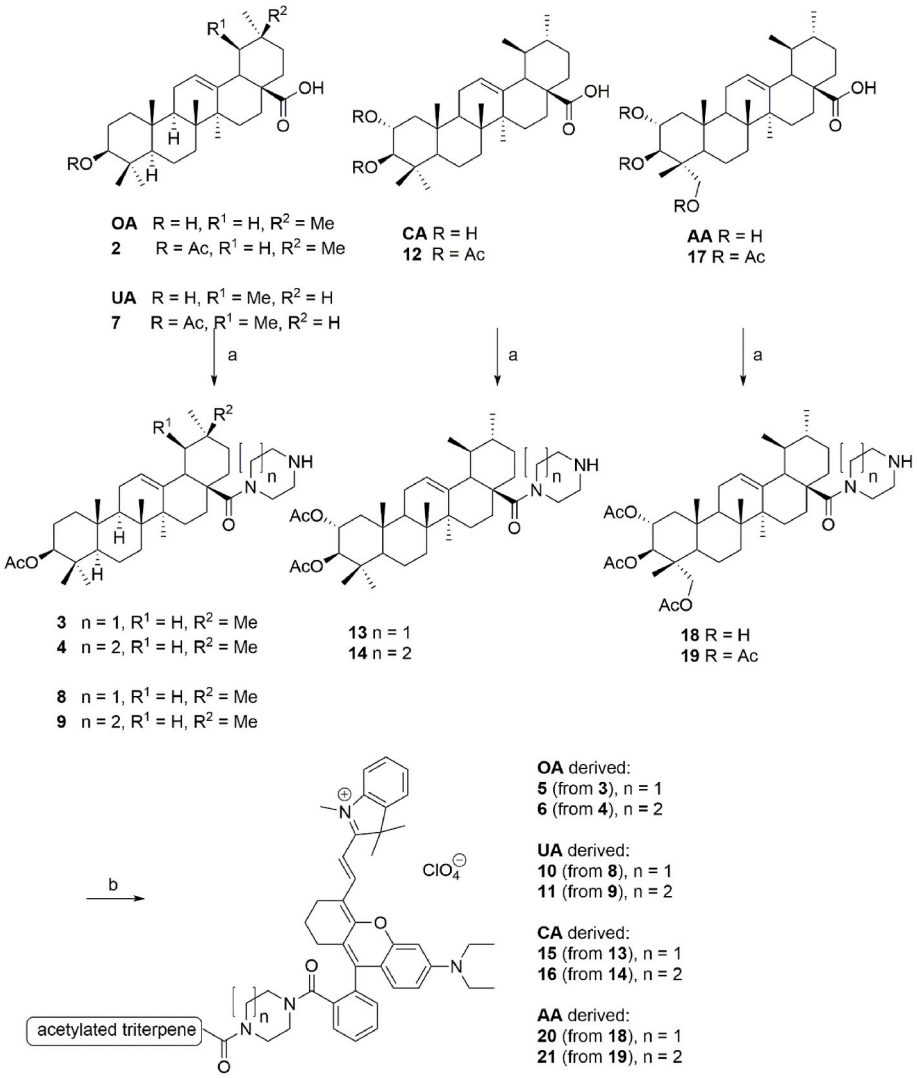

Scheme 2. Synthesis of the (homo)-piperazinyl spacered triterpenoic acid CS-2 hybrids; reactions and conditions: a) $(COCl)_2$, DMF (cat.), DCM, 1 h; b) **1**, DCM, $(COCl)_2$, DMF (cat), 23 °C, 1h, then acetylated triterpene (homo)-piperazinyl amide, DCM, NEt_3, 1 d, 23 °C.

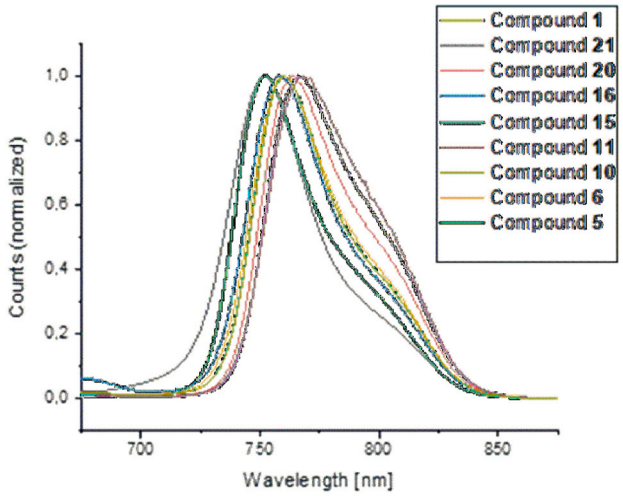

Fig. 3. Mission spectra of parent dye CS-2 (**1**) and spacered triterpenoic acid CS-2 hybrids **5**, **6**, **10**, **11**, **15**, **16**, **20**, and **21** (in MeOH solution; excitation wavelengths λ = 500/430 nm).

including standard deviations were carried out using GraphPad Prism8.

4.4. Staining

Analysis of subcellular localization of compounds was performed in A549 cells using the mitochondrial targeting compound BioTracker™ 488 Green Mitochondria Dye (Sigma-Aldrich Chemie GmbH, Taufkirchen, Germany) and the established compound **AAHR** for comparison. Cells were seeded in a µ-Plate 96 Well Black plate (ibiTreat: #1.5 polymer coverslip bottom, ibidi GmbH, Gräfelfing, Germany) at cell density of 30.000 per well. After 24h cells were treated with 20 nM of compounds for 24h or 100 nM BioTracker488 for 30min, followed by rinsing and supplementation with RPMI 1640 w/o Phenol-red (PanBiotech GmbH, Aidenbach, Germany). For simultaneous analysis of subcellular localization, cells were treated with 20 nM of compounds for 24h followed by 30min treatment with BioTracker 488 and Hoechst 33342 (Sigma-Aldrich). Live cell imaging was performed on an Axio Observer 7 (Carl Zeiss Microscopy Deutschland GmbH, Oberkochen, Germany) using the settings for Ex/Em as followed: Hoechst 33342 (385nm/425 nm), BioTracker (475nm/514 nm), **AAHR** (555nm/592 nm), CS2-compounds (735nm/785 nm). For simultaneous analysis, multiple Z-stacked images were taken and resulting pictures were reconstructed using the ZEN 3.5 pro software (Zeiss).

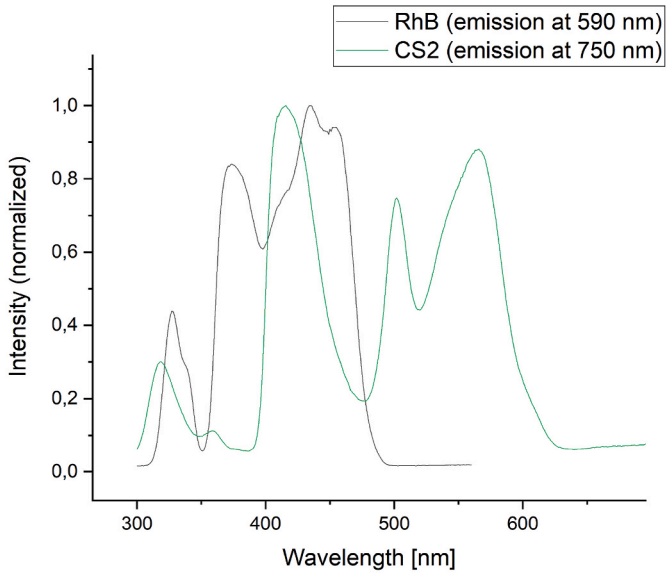

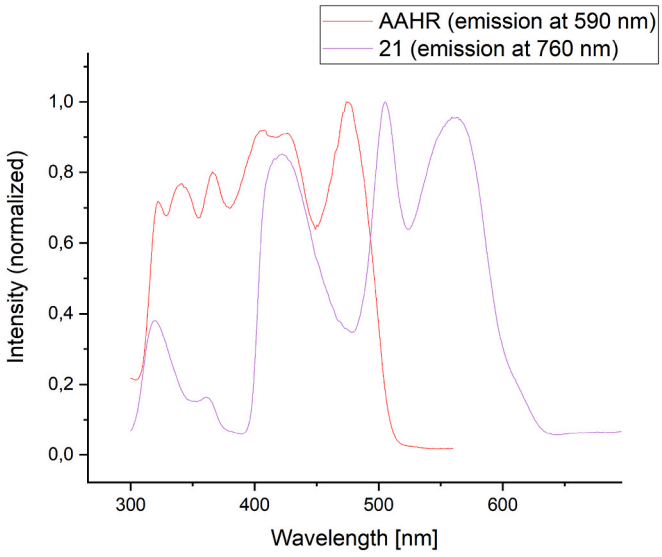

Fig. 4. Comparison maximum excitation wavelengths (vs normalized intensity) of rhodamine B and CS-2 (**1**, top) and a rhodamine B hybrid (**AAHR**) and the corresponding CS-2 conjugate **21** (bottom).

*4.5. General procedure for the synthesis of acetates **2, 7, 12 and 17** (GPA)*

To a solution of the triterpenoic acid (**OA**, **UA**, **CA**, **AA**) in DCM, acetic anhydride (3 equiv.), triethylamine (3 equiv.), and DMAP (cat.) were added, and the mixture was stirred at room temperature for 24 h. Usual aqueous work-up followed by re-crystallization from ethanol gave products **2, 7, 12 and 17**.

4.6. General procedure for the synthesis of acetylated (homo)piperazinyl amides (GPB)

To a solution of the acetylated triterpenoic acid **2,7, 12 and 17** (1 equiv.) in dry DCM, DMF (cat.) and oxalyl chloride (4 equiv.) were added, and the reaction mixture was allowed to stir until the evolution of volatiles had ceased (about 1 h). The volatiles were removed under reduced pressure, and the residue was re-dissolved in dry THF, and the solvent was removed again under reduced pressure. The triterpenoic

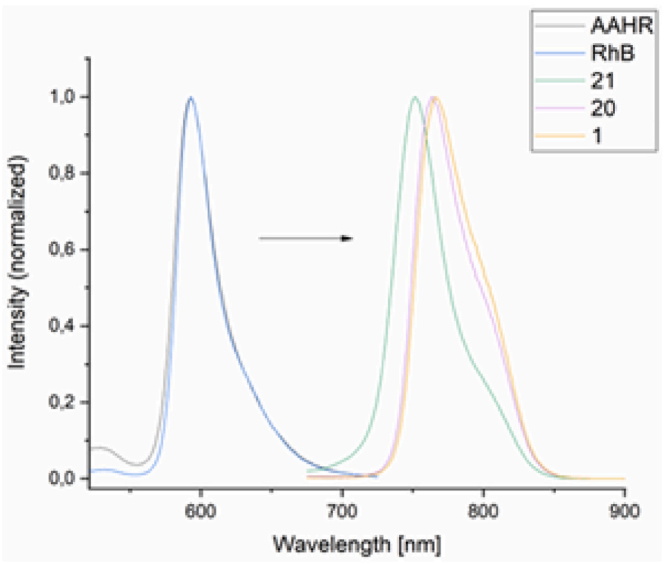

Fig. 5. Comparison emitted light in rhodamine B and CS-2 hybrids.

acyl chloride was dissolved in dry DCM and added dropwise to a solution of the amine (4 equiv.) in dry DCM. After stirring for 1h at room temperature, followed by usual aqueous work-up and column chromatography, products **3/4, 8/9, 13/14** and **18/19** were obtained.

4.7. General procedure for the synthesis of the rhodamine conjugates (GPC)

The acyl chloride was prepared as described (GPB) above starting from **1**. This acid chloride was slowly added to the solution of the respective triterpenoic amide (1.25 eq. in DCM) in the presence of triethylamine (2 eq.). After stirring for 1 day at room temperature, the crude product was purified by column chromatography to yield **5/6**, **10/11**, **15/16** and **20/21**, respectively.

4.8. Syntheses

*4.8.1. 2-[(1E)-2-[9-(2-carboxyphenyl)-6-(diethylamino)-2,3-dihydro-1H-xanthen-4-yl]ethenyl]-1,3,3-trimethyl-3H-indolium perchlorate (**1**) [20]*

A solution of cyclohexanone (6.6 mL, 64.0 mmol) in concentrated sulphuric acid (80 mL) was cooled to 0 °C, 2-(4-(diethylamino)-2-hydroxybenzoyl)-benzoic acid (10.0 g, 32.0 mmol) was added, and the reaction mixture was heated at 90 °C for 90 min. After cooling to room temperature, the reaction mixture was poured into ice cold water, perchloric acid (70%, 10 mL) was added, and the precipitate was filtered off. It was redissolved in acetic anhydride (250 mL). (*Z*)-2-(1,3,3-trimethylindolin-2-ylidene)-acetaldehyde (6.4 g, 32 mmol) was added, and the mixture was stirred at 50 °C for 30 min. After quenching with water (100 mL), the solvents were removed under reduced pressure; purification by column chromatography ($CHCl_3$/MeOH, 95:5) gave **1** (10.5 g, 50%) as a dark green solid; m.p. >300 °C (decomp.); $R_F = 0.11$ (SiO_2, $CHCl_3$/MeOH, 95:5); UV–Vis (MeOH): λ_{max} (log ε) = 293 nm (4.75), 387 nm (4.78), 474 nm (4.45), 654 nm (4.75), 706 nm (5.18); IR (ATR): ν = 2931*w*, 1721*w*, 1624*w*, 1575*w*, 1549*w*, 1528*w*, 1438*s*, 1399*w*, 1365 *m*, 1309 *m*, 1268 *m*, 1248*s*, 1223 *m*, 1167 *m*, 1142 *m*, 1099*s*, 1062*s*, 1040*s*, 1016*s*, 994 *m*, 924 *m*, 859*w*, 814 *m*, 796 *m*, 748 *m*, 710*w*, 675*w*, 621 m cm^{-1}; ^1H NMR (400 MHz, $CDCl_3$): δ = 8.56 (d, *J* = 14.1 Hz, 1H, 25-H), 8.22 (d, *J* = 7.0 Hz, 1H, 3-H), 7.71 (*dd*, *J* = 7.5-H, 1.2 Hz, 1H, 5-H), 7.58 (dd, *J* = 7.8 Hz, 1.2 Hz, 1H, 4-H), 7.41 (dd, *J* = 7.4 Hz, 0.6 Hz, 1H, 30-H), 7.36 (*td*, *J* = 7.8 Hz, 1.1 Hz, 1H, 31-H), 7.22 (d, *J* = 7.4 Hz, 1H, 32-H), 7.15 (s, 1H, 13-H), 7.13 (s, 1H, 6-H), 6.67 (d, *J* = 9.1 Hz, 1H, 33-H), 6.60 (d, *J* = 2.2 Hz, 1H, 10-H), 6.57 (d, *J* = 3.1 Hz,

Table 1
SRB cytotoxicity assay: IC_{50} values [nM] after 72 h of treatment; averaged from three to four independent experiments (excepting **1**: n = 1). Human cancer cell lines: A2780 (ovarian carcinoma), A2780cis (resistant derivative of A2780), A549 (lung carcinoma), HT29 (colorectal carcinoma), MCF7 (breast carcinoma), CCD18Co (non-malignant human fibroblasts). Doxorubicin (**Dox**) has been used as a positive standard. Resistance index (RI): IC_{50} ratio of A2780cis/A2780, Selectivity index 1 (SI 1): IC_{50} ratio of CCD18Co/A2780, Selectivity index 2 (SI 2): IC_{50} ratio of CCD18Co/MCF7.

#	A2780	A2780CIS	A549	HT29	MCF7	CCD18CO	RI	SI 1	SI 2
5	102.2 ± 21.2	203.2 ± 43.5	151.4 ± 12.2	268.1 ± 47.8	530.4 ± 82.0	1229.0 ± 668.0	2.0	12.0	2.3
6	32.8 ± 14.4	116.6 ± 55.0	58.5 ± 20.8	158.2 ± 24.8	336.9 ± 64.6	250.6 ± 135.4	3.6	7.6	0.7
10	123.0 ± 19.3	223.3 ± 33.7	210.1 ± 29.3	376.8 ± 59.0	495.8 ± 69.7	606.7 ± 253.9	1.8	4.9	1.2
11	73.2 ± 3.3	166.8 ± 35.9	86.2 ± 18.0	233.1 ± 13.2	418.0 ± 49.5	256.0 ± 138.5	2.3	3.5	0.6
15	33.2 ± 7.1	75.4 ± 34.2	87.5 ± 19.5	127.7 ± 16.0	147.4 ± 42.0	441.6 ± 252.0	2.3	13.3	3.0
16	7.7 ± 2.3	25.2 ± 11.4	34.8 ± 6.5	49.3 ± 18.7	77.6 ± 3.6	375.3 ± 274.8	3.3	49.0	4.8
20	3.5 ± 0.0	6.7 ± 0.0	17.0 ± 8.5	11.3 ± 5.6	19.9 ± 5.1	118.8 ± 46.3	1.9	34.0	6.0
21	1.1 ± 0.3	3.1 ± 0.5	5.6 ± 0.6	5.2 ± 1.9	12.9 ± 1.5	64.1 ± 22.1	2.9	58.6	5.0
1	1514.0	1140.0	1578.0	1838.0	1273.0	6505.0	0.8	4.3	5.1
Dox	8.5 ± 2.4	80.4 ± 24.6	21.5 ± 4.1	107.8 ± 33.0	34.2 ± 1.8	757.1 ± 166.7	9.4	88.8	22.2

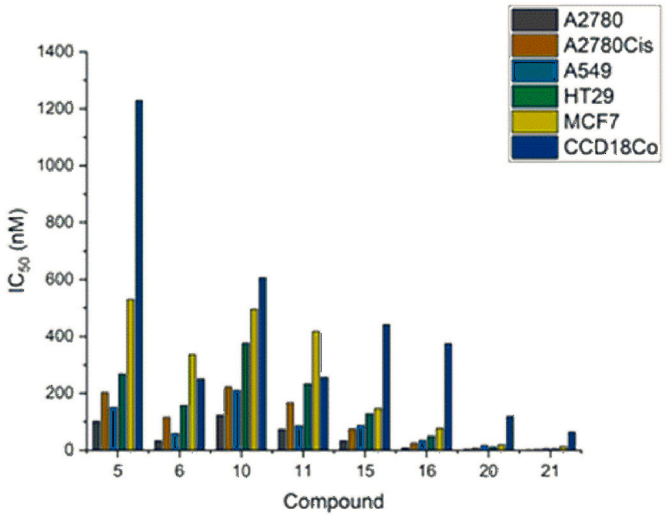

Fig. 6. Cytotoxicity (IC_{50} values, nM) of CS-2 triterpene conjugates for different cancer cell lines (A2780, A2780cis, A549, HT29, MCF7) as well as non-malignant human fibroblasts CCD18Co.

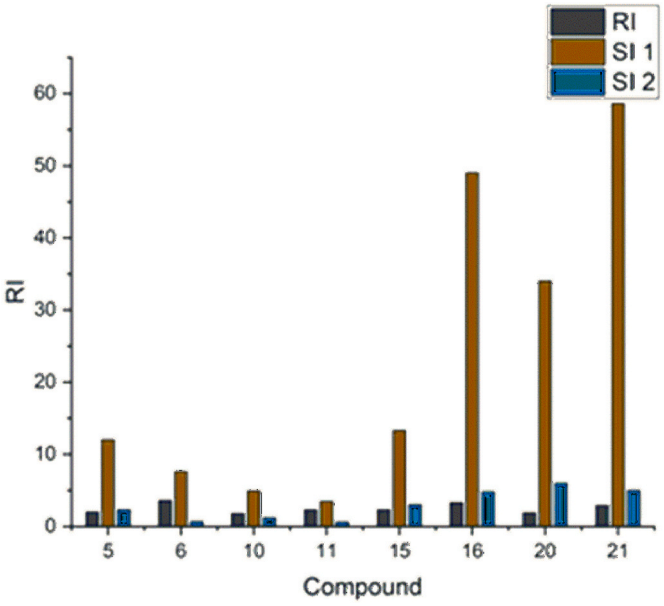

Fig. 7. Comparison of resistance/selectivity index values for the CS-2 hybrids; selectivity index 1 (SI 1): IC_{50} ratio of CCD18Co/A2780, selectivity index 2 (SI 2): IC_{50} ratio of CCD18Co/MCF7; RI (resistance index): IC_{50} ratio of A2780cis/A2780.

1H, 11-H), 6.05 (d, J = 14.1 Hz, 1H, 26-H), 3.65 (s, 3H, 37-H), 3.50 (q, J = 7.1 Hz, 4H, 21-H, 22-H), 2.64 (t, J = 5.8 Hz, 2H, 19-H), 2.30–2.22 (m, 2H, 17-H), 1.78 (s, 3H, 36-H), 1.77 (s, 3H, 35-H), 1.84–1.70 (m, 2H, 18-H), 1.25 (t, J = 7.1 Hz, 6H, 23-H, 24-H) ppm; ^{13}C NMR (101 MHz, $CDCl_3$): δ = 173.3 (C-27), 168.5 (C-1), 163.4 (C-14), 156.0 (C-8), 152.3 (C-15), 152.1 (C-12), 143.0 (C-34), 142.1 (C-25), 140.7 (C-29), 136.3 (C-7), 133.5 (C-5), 132.0 (C-3), 129.5 (C-6), 129.5 (C-4), 129.1 (C-2), 128.8 (C-31), 128.3 (C-30), 125.2 (C-32), 122.3 (C-33), 121.2 (C-20), 116.0 (C-16), 113.6 (C-9), 112.4 (C-10), 110.6 (C-13), 99.5 (C-26), 96.0, 49.3 (C-28), 45.3 (C-21, 22), 31.7 (C-37), 28.6 (C-35, C-36), 26.7 (C-17), 24.3 (C-19), 20.6 (C-18), 12.6 (C-23, C-24) ppm; MS (ESI, MeOH/$CHCl_3$, 4:1): m/z = 559.2 (100%, $[M]^+$); anal. Calcd for $C_{37}H_{39}N_2O_7Cl$ (659.18), C 67.42, H 5.96, N 4.25; found: C 67.23, H 6.13, N 4.01.

*4.8.2. 3β-Acetyloxy-olean-12-en-oic acid (**2**)*

Following GPA, compound **2** (1.24 g, 92%) was obtained from **OA** as a colorless solid; R_F = 0.70 (toluene/ethyl acetate/heptane/formic acid, 80:26:10:5); m.p. 285–287 °C (lit.: 286–289 °C [6]); $[\alpha]_D^{20}$ = +66.1° (c 0.20, $CHCl_3$) (lit.: $[\alpha]_D^{20}$ = +69.4° (c 0.30, $CHCl_3$) [6]); MS (ESI, MeOH): m/z (%) = 499.2 ([100%, M + H]$^+$).

*4.8.3. 3β-Acetyloxy-28-(1-piperazinyl)-olean-12-en-28-one (**3**)*

Following GPB from **2** (4.0 g, 8.0 mmol) and piperazine (2.8 g, 32.0 mmol), **3** (3.95 g, 87%) was obtained as a colorless solid; R_F = 0.12 (SiO_2, $CHCl_3$/MeOH, 95:5); m.p. = 173–175 °C (lit.: 172–175 °C [6]); $[\alpha]_D^{20}$ = +28.0° (c 0.26, $CHCl_3$), (lit.: $[\alpha]_D^{20}$ = +23.4° (c 0.18, $CHCl_3$) [6]); MS (ESI, MeOH): m/z (%) = 567.3 (100%, $[M + H]^+$).

*4.8.4. 3β-Acetyloxy-28-(1-homopiperazinyl)-olean-12-en-28-one (**4**)*

Following GPB from **2** (4.0 g, 8.0 mmol) and homopiperazine (3.2 g, 32.0 mmol), **4** (4.2 g, 91%) was obtained as a colorless solid; R_F = 0.12 (SiO_2, $CHCl_3$/MeOH, 95:5); m.p. 183–185 °C (lit.: 182–185 °C [6]); $[\alpha]_D^{20}$ = 12.0° (c 0.14, $CHCl_3$), (lit.: $[\alpha]_D^{20}$ = +12.4° (c 0.14, $CHCl_3$) [6]); MS (ESI, MeOH): m/z (%) = 581.3 (100%, $[M + H]^+$).

*4.8.5. (E)-2-(2-[6-(diethylamino)-9-[2-[4-[3β-Acetyloxy-28-oxo-olean-12-en-28-ylpiperazine-1-carbonyl]phenyl]-2,3-dihydro-1H-xanthen-4-yl] vinyl)-1,3,3-trimethyl-3H-indol-1-ium perchlorate (**5**)*

Following GPC from **3** (283 mg, 0.5 mmol) and **1** (250 mg, 0.38 mmol), **5** (280 mg, 61%) was obtained as a green solid; m.p. >300 °C (decomp.); R_F = 0.10 (SiO_2, $CHCl_3$/MeOH, 95:5); UV–Vis (MeOH): λ_{max} (log ε) = 296 nm (4.41), 385 nm (4.44), 477 nm (4.23), 659 nm (4.71), 715 nm (5.08); IR (ATR): ν = 2928*w*, 1728*w*, 1624 *m*, 1578*w*, 1551*w*, 1440 *m*, 1400*w*, 1365 *m*, 1309*w*, 1268*w*, 1247*s*, 1226 *m*, 1167 *m*, 1143 *m*, 1096*s*, 1064*s*, 1043 *m*, 1000 *m*, 925 *m*, 860*w*, 811 *m*, 747 *m*, 671*w*, 622 m cm^{-1}; ^{1}H NMR (500 MHz, $CDCl_3$): δ = 8.58 (d, J = 13.7 Hz, 1H,

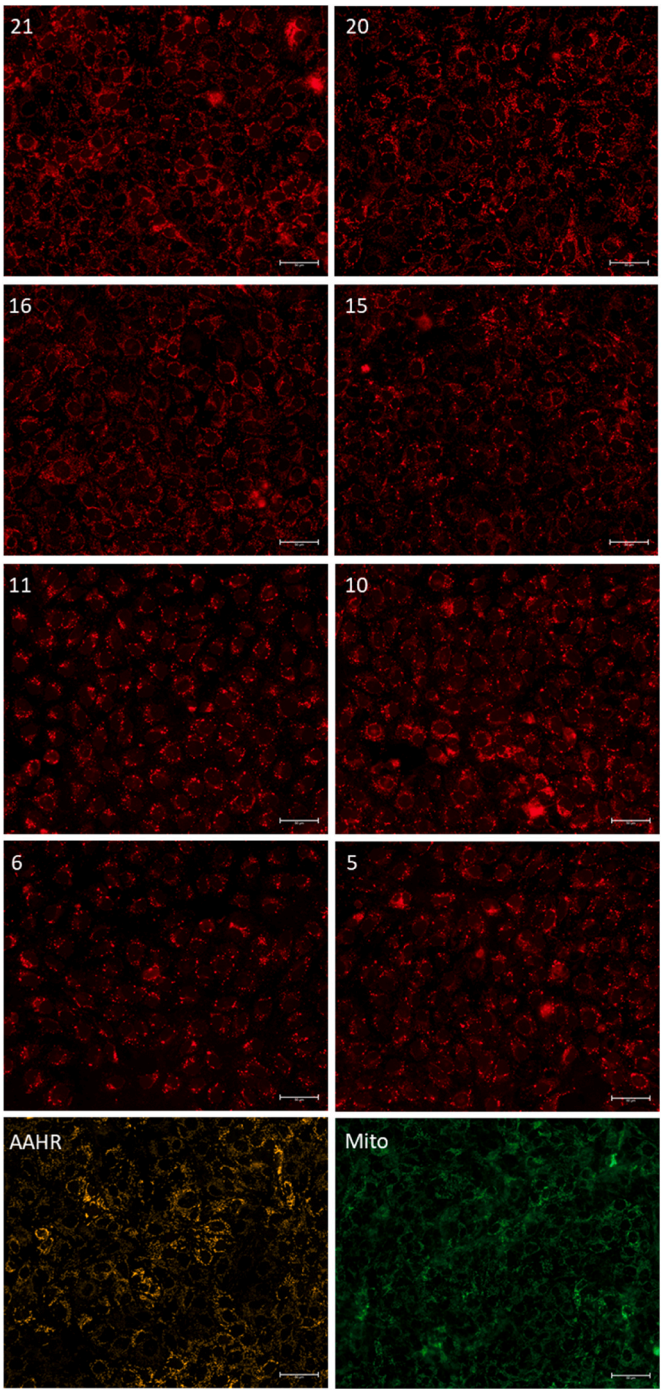

Fig. 8. Analysis of subcellular localization of CS2-compounds compared to the mitochondrial targeting compound BioTracker™ 488 Green Mitochondria Dye (Mito, lower right) and **AAHR** (lower, left) in A549 cells showing different pattern of accumulation among CS2-compounds, with **16**, **20** and **21** most resembling those of BioTracker and **AAHR**, indicating mitochondrial targeting. Scale bar: 50 μm; for higher resolution see original images in Supplementary Materials File.

57-H), 7.62–7.54 (m, 2H, 39-H, 40-H), 7.46–7.36 (m, 3H, 41-H, 42-H, 61-H), 7.28–7.17 (m, 3H, 52-H, 62-H, 64-H), 6.81 (dd, J = 18.3 Hz, 9.1 Hz, 1H, 63-H), 6.76–6.65 (m, 1H, 55-H), 6.55 (dd, J = 9.4 Hz, 2.0 Hz, 1H, 54-H), 6.07 (t, J = 13.1 Hz, 1H, 58-H), 5.22 (s, 1H, 12-H), 4.49–4.45 (m, 1H, 3-H), 3.71 (d, J = 7.0 Hz, 3H, 67-H), 3.54–3.47 (m, 4H, 70-H, 72-H), 3.46–3.05 (m, 8H, 33-H, 34-H, 35-H, 36-H), 3.00 (d, J = 15.3 Hz, 1H, 18-H), 2.71–2.61 (m, 2H, 46-H), 2.57–2.46 (m, 1H, 16-H_b), 2.40–2.28 (m, 1H, 16-H_a), 2.14–2.05 (m, 1H, 2-H_a), 2.03 (s, 3H, 32-H), 1.93–1.81 (m, 4H, 11-H, 47-H), 1.78 (s, 3H, 69-H), 1.78 (s, 3H, 68-H), 1.75–1.30 (m, 13H, 1-H_a, 2-H_b, 6-H, 7-H_a, 9-H, 15-H_a, 19-H_a, 21-H, 22-H_a, 48-H), 1.28–1.22 (m, 6H, 71-H, 73-H), 1.10 (s, 3H, 27-H), 1.19–0.98 (m, 5H, 1-H_b, 7-H_b, 15-H_b, 19-H_b, 22-H_b), 0.90–0.89 (m, 3H, 25-H), 0.87 (s, 3H, 30-H), 0.86 (s, 3H, 29-H), 0.85 (s, 3H, 23-H), 0.83 (s, 3H, 24-H), 0.83–0.78 (m, 1H, 5-H), 0.67 (s, 3H, 26-H) ppm; ^{13}C NMR (126 MHz, $CDCl_3$): δ = 175.8 (C-28), 174.1 (C-59), 171.1 (C-31), 168.2 (C-37), 163.0 (C-51), 155.8 (C-44), 152.1 (C-53), 152.1 (C-50), 144.8 (C-13), 142.9 (C-60), 142.7 (C-57), 140.8 (C-65), 134.5 (C-43), 133.3 (C-38), 130.3 (C-42), 129.7 (C-41), 129.6 (C-39), 129.3 (C-40), 129.0 (C-63), 127.6 (C-64), 125.6 (C-62), 122.7 (C-45), 122.4 (C-61), 121.6 (C-12), 116.0 (C-49), 113.5 (C-56), 112.1 (C-55), 110.9 (C-52), 99.9 (C-58), 96.0 (C-54), 81.0 (C-3), 55.4 (C-5), 49.5 (C-17), 47.8 (C-9), 47.6 (C-66), 47.1 (C-33, 36), 46.8 (C-34, 35), 46.4 (C-19), 45.3 (C-70, 72), 43.7 (C-18), 42.0 (C-14), 39.2 (C-8), 38.2 (C-1), 37.8 (C-10), 37.1 (C-4), 34.0, 33.1 (C-29), 32.9 (C-7), 31.9 (C-67), 30.4 (C-20), 30.1 (C-48), 29.9 (C-21), 28.5 (C-23), 28.2 (C-68, C-69), 27.9 (C-15), 27.2 (C-16), 26.0 (C-27), 24.4 (C-46), 24.1 (C-30), 23.6 (C-11), 23.5 (C-2), 21.4 (C-32), 20.7 (C-47), 18.3 (C-6), 17.0 (C-24), 16.8 (C-26), 15.5 (C-25), 12.6 (C-71, C-73) ppm; MS (ESI, MeOH/$CHCl_3$, 4:1): m/z (%) = 1108.2 (100%, $[M]^+$); anal. calcd for $C_{73}H_{95}N_4O_9Cl$ (1208.03), C 72.58, H 7.93, N 4.64; found: C 72.39, H 8.07, N 4.42.

4.8.6. (E)-2-(2-[6-(diethylamino)-9-[2-[4-[3β-Acetyloxy-28-oxo-olean-12-en-28-ylhomopiperazine-1-carbonyl]phenyl]-2,3-dihydro-1H-xanthen-4-yl]vinyl)-1,3,3-trimethyl-3H-indol-1-ium perchlorate (6)

Following GPC from **4** (290 mg, 0.5 mmol) and **1** (250 mg, 0.38 mmol), **6** (225 mg, 49%) was obtained as a green solid; m.p. >300 °C (decomp.); R_F = 0.10 (SiO_2, $CHCl_3$/MeOH, 95:5); UV–Vis (MeOH): λ_{max} (log ε) = 300 nm (4.09), 391 nm (4.23), 478 nm (3.79), 659 nm (4.47), 718 nm (4.83); IR (ATR): ν = 2939*w*, 1729*w*, 1624 *m*, 1577*w*, 1551*w*, 1441 *m*, 1401*w*, 1365 *m*, 1309*w*, 1268*w*, 1247*s*, 1227 *m*, 1247*s*, 1227 *m*, 1168 *m*, 1143 *m*, 1104*s*, 1065*s*, 1043 *m*, 925 *m*, 860*w*, 811 *m*, 748 *m*, 670*w*, 622 m cm^{-1}; ^{1}H NMR (500 MHz, $CDCl_3$): δ = 8.57 (d, J = 13.9 Hz, 1H, 58-H), 7.59–7.47 (m, 2H, 40-H, 41-H), 7.48–7.34 (m, 3H, 42-H, 43-H, 63-H), 7.25–7.15 (m, 3H, 53-H, 62-H, 65-H), 6.87–6.77 (m, 1H, 64-H), 6.70–6.48 (m, 2H, 55-H, 56-H), 6.07 (dd, J = 39.5 Hz, 13.7 Hz, 1H, 59-H), 5.33–5.17 (m, 1H, 12-H), 4.47 (t, J = 7.2 Hz, 1H, 3-H), 3.74–3.68 (m, 3H, 68-H), 3.58–3.43 (m, 4H, 71-H, 72-H), 3.88–3.03 (m, 8H, 33-H, 34-H, 35-H, 37-H), 2.64 (s, 2H, 47-H), 2.32 (s, 3H, 16-H, 18-H), 2.11 (s, 1H, 2-H_b), 2.03 (s, 3H, 32-H), 1.97–1.81 (m, 5H, 11-H, 15-H_b, 49-H), 1.78 (s, 3H, 70-H), 1.77 (s, 3H, 69-H), 1.70–1.32 (m, 14H, 1-H_b, 2-H_a, 6-H, 7-H_b, 9-H, 19-H_b, 21-H, 22-H_b, 36-H, 48-H), 1.26 (q, J = 6.8 Hz, 6H, 73-H, 74-H), 1.10 (s, 3H, 27-H), 1.21–0.99 (m, 5H, 1-H_a, 7-H_a, 15-H_a, 19-H_a, 22-H_a), 0.91 (s, 3H, 30-H), 0.90 (s, 3H, 25-H), 0.86 (s, 3H, 29-H), 0.84 (s, 3H, 23-H), 0.83 (s, 3H, 24-H), 0.82–0.79 (m, 1H, 5-H), 0.70 (s, 3H, 26-H) ppm; ^{13}C NMR (126 MHz, $CDCl_3$): δ = 176.4 (C-28), 174.5 (C-60), 171.1 (C-31), 169.1 (C-38), 163.2 (C-52), 155.9 (C-45), 152.2 (C-51), 152.1 (C-54), 144.9 (C-13), 143.0, 142.9 (C-58, 61), 140.8 (C-66), 135.5 (C-44), 132.6 (C-39), 129.8 (C-43), 129.6 (C-42), 129.1 (C-41), 129.0 (C-40), 128.9 (C-64), 126.8 (C-65), 125.6 (C-63), 122.8 (C-46), 122.3 (C-62), 121.5 (C-12), 116.1 (C-50), 113.6 (C-57), 111.8 (C-56), 110.9 (C-53), 99.9 (C-59), 95.8 (C-55), 81.1 (C-3), 55.5 (C-5), 49.5 (C-17), 47.9 (C-67), 47.8 (C-9), 46.8 (C-37), 46.7 (C-33), 46.7, 46.6 (C-19), 46.5 (C-35), 46.5 (C-34), 45.3 (C-71, C-72), 45.2, 43.7 (C-18), 42.1 (C-14), 39.2 (C-8), 38.2 (C-1), 37.8 (C-10), 37.1 (C-4), 34.2 (C-22), 33.2 (C-29), 32.9 (C-7), 32.0 (C-68), 30.5 (C-20), 29.8 (C-36), 29.8 (C-48), 29.2 (C-21), 28.5 (C-23), 28.1 (C-69, 70), 28.0 (C-15), 27.1 (C-16), 25.9 (C-27), 24.4 (C-47), 24.2 (C-30), 23.6 (C-2), 23.5 (C-11), 21.4 (C-32), 20.6 (C-49), 18.3 (C-6), 17.1 (C-24), 16.8 (C-26), 15.5 (C-25), 12.6 (C-73, 74) ppm; MS (ESI, MeOH/$CHCl_3$, 4:1): m/z (%) = 1122.1 (100%, $[M]^+$); anal. calcd for $C_{74}H_{97}N_4O_9Cl$ (1222.06), C 72.73, H 8.00, N 4.58; found: C 72.50, H 8.29, N 4.19.

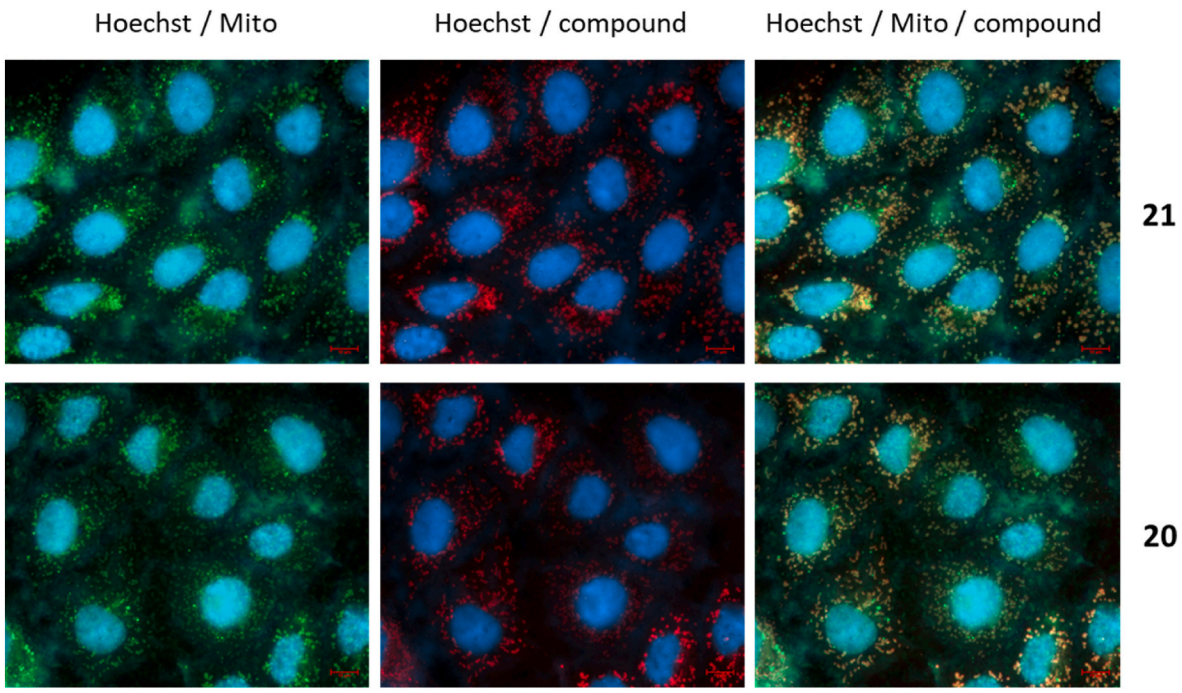

Fig. 9. Analysis of subcellular localization of **20** and **21** using combined treatment with the mitochondrial targeting compound BioTracker™ 488 Green Mitochondria Dye (Mito) and Hoechst 33342 for staining of nuclei confirming mitochondrial localization of compounds. Scale bar: 10 μm; (for higher resolution see original images in Supplementary Materials File).

4.8.7. 3β-Acetyloxy-urs-12-en-oic acid (7)

Following GPA, compound **7** (1.62 g, 94%) was obtained from **UA** as a colorless solid; R_F = 0.68 (*n*-hexane/ethyl acetate, 7:3); m.p. 281–283 °C (lit.: 281–283 °C [6]); $[\alpha]_D$ = +64.2° (*c* 0.15, $CHCl_3$) (lit.: $[\alpha]_D^{20}$ = +66.5° (*c* 0.42, $CHCl_3$) [6]); MS (ESI, MeOH): *m/z* (%) = 499.3 (100%, $[M + H]^+$).

4.8.8. 3β-Acetyloxy-28-(1-piperazinyl)-urs-12-en-28-one (8)

Following GPB from **7** (2.5 g, 5.0 mmol) and piperazine (1.6 g, 20.0 mmol), **7** (2.44 g, 86%) was obtained as a colorless solid; R_F = 0.11 (SiO_2, $CHCl_3$/MeOH, 95:5); m.p. = 188–190 °C (lit.: 187–190 °C [6]); $[[\alpha]_D^{20}$ = +27.2° (*c* 0.10, MeOH), (lit.: $[\alpha]_D^{20}$ = +25.1° (*c* 0.24, MeOH) [6]); MS (ESI, MeOH): *m/z* (%) = 567.4 (100%, $[M + H]^+$).

4.8.9. 3β-Acetyloxy28-(1-homopiperazinyl)-urs-12-en-28-one (9)

Following GPB from **7** (1.0 g, 2.0 mmol) and homopiperazine (1.6 g, 16.0 mmol), **9** (2.0 g, 86%) was obtained as a colorless solid; R_F = 0.12 (SiO_2, $CHCl_3$/MeOH, 95:5); m.p. 172–175 °C (lit.: 171–175 °C [6]); $[\alpha]_D^{20}$ = +31.1° (*c* 0.15, $CHCl_3$), (lit.: $[\alpha]_D^{20}$ = +27.0° (*c* 0.21, $CHCl_3$) [6]); MS (ESI, MeOH): *m/z* (%) = 581.4 (100%, $[M + H]^+$).

4.8.10. (E)-2-(2-[6-(diethylamino)-9-[2-[4-[3β-Acetyloxy-28-oxo-ursan-12-en-28-ylpiperazine-1-carbonyl]phenyl]-2,3-dihydro-1H-xanthen-4-yl] vinyl)-1,3,3-trimethyl-3H-indol-1-ium perchlorate (10)

Following GPC from **8** (283 mg, 0.5 mmol) and **1** (250 mg, 0.38 mmol), **10** (240 mg, 52%) was obtained as a green solid; m.p. >300 °C (decomp.); R_F = 0.10 (SiO_2, $CHCl_3$/MeOH, 95:5); UV–Vis (MeOH): λ_{max} (log ε) = 298 nm (4.38), 390 nm (4.42), 477 nm (4.08), 659 nm (4.68), 717 nm (5.04); IR (ATR): ν = 2925*w*, 1729*w*, 1624 *m*, 1577*w*, 1551*w*, 1440 *m*, 1399*w*, 1365 *m*, 1309*w*, 1268*w*, 1247*s*, 1227 *m*, 1167 *m*, 1143 *m*, 1095*s*, 1065*s*, 1043 *m*, 1004 *m*, 925 *m*, 860*w*, 811 *m*, 748 *m*, 672*w*, 622 m cm^{-1}; ^1H NMR (500 MHz, $CDCl_3$): δ = 8.57 (d, *J* = 14.1 Hz, 1H, 57-H), 7.63–7.53 (m, 2H, 39-H, 40-H), 7.47–7.34 (m, 3H, 41-H, 42-H, 61-H), 7.25–7.16 (m, 3H, 52-H, 62-H, 64-H), 6.81 (t, *J* = 9.1 Hz, 1H, 63-H), 6.75–6.64 (m, 1H, 55-H), 6.54 (s, 1H, 54-H), 6.07 (dd, *J* = 14.0 Hz, 8.1 Hz, 1H), 5.24–5.11 (m, 1H, 12-H), 4.53–4.42 (m, 1H, 3-H), 3.70 (d, *J* = 3.9 Hz, 3H, 67-H), 3.50 (q, *J* = 7.0 Hz, 4H, 70-H, 72-H), 3.64–3.20 (m, 8H, 33-H, 34-H, 35-H, 36-H), 2.68–2.62 (m, 2H, 46-H), 2.58–2.46 (m, 1H, 16-H_b), 2.39–2.25 (m, 3H, 16-H_a, 48-H), 2.03 (s, 3H, 32-H), 1.78 (s, 6H, 68-H, 69-H), 1.94–1.66 (m, 5H, 11-H, 22-H_b, 47-H), 1.64–1.28 (m, 14H, 1-H_a, 2-H, 6-H, 7-H, 9-H, 15-H_a, 18-H, 19-H, 21-H, 22-H_a), 1.25 (t, *J* = 7.1 Hz, 6H, 71-H, 73-H), 1.04 (s, 3H, 27-H), 0.92–0.90 (m, 6H, 25-H, 29-H), 0.88 (s, 4H, 1-H_b, 5-H, 15-H_b, 20-H), 0.86–0.83 (m, 6H, 24-H, 30-H), 0.83 (s, 3H, 23-H), 0.67 (s, 3H, 26-H) ppm; ^{13}C NMR (126 MHz, $CDCl_3$): δ = 176.0 (C-28), 174.1 (C-59), 171.1 (C-31), 168.2 (C-37), 163.0 (C-51), 155.8 (C-44), 152.1 (C-53), 152.0 (C-50), 142.9 (C-60), 142.8 (C-57), 140.8 (C-13), 140.8 (C-65), 134.5 (C-43), 133.2 (C-38), 130.3 (C-42), 129.7 (C-41), 129.2 (C-39), 129.2 (C-40), 128.9 (C-63), 127.6 (C-64), 125.6 (C-62), 125.2 (C-12), 122.7 (C-45), 122.3 (C-61), 116.0 (C-49), 113.3 (C-56), 112.1 (C-55), 110.9 (C-52), 100.1 (C-58), 96.1 (C-54), 81.0 (C-3), 77.4, 77.2, 76.9, 55.4 (C-5), 49.5 (C-17), 48.7 (C-33, 36), 47.7 (C-18), 47.6 (C-9), 47.4 (C-34, 35), 46.5 (C-66), 45.3 (C-70, 72), 42.0 (C-14), 39.4 (C-19), 38.8 (C-20), 38.3 (C-1), 37.8 (C-8), 37.1 (C-4), 37.0 (C-10), 34.4 (C-22), 32.9 (C-7), 31.9 (C-67), 30.5 (C-21), 28.5 (C-68, C-69), 28.2 (C-15), 28.2 (C-23), 27.9 (C-48), 27.1 (C-16), 24.4 (C-46), 24.1 (C-27), 23.6 (C-11), 23.4 (C-2), 21.4 (C-32), 21.3 (C-29), 20.6 (C-47), 18.3 (C-6), 17.5 (C-30), 17.0 (C-26), 16.8 (C-24), 15.6 (C-25), 12.6 (C-71), 12.6 (C-73) ppm; MS (ESI, MeOH/$CHCl_3$, 4:1): *m/z* (%) = 1108.2 (100%, $[M]^+$); anal. calcd for $C_{73}H_{95}N_4O_9Cl$ (1208.03), C 72.58, H 7.93, N 4.64; found: C 72.39, H 8.12, N 4.40.

4.8.11. (E)-2-(2-[6-(diethylamino)-9-[2-[4-[3β-Acetyloxy-28-oxo-ursan-12-en-28-ylhomopiperazine-1-carbonyl]phenyl]-2,3-dihydro-1H-xanthen-4-yl]vinyl)-1,3,3-trimethyl-3H-indol-1-ium perchlorate (11)

Following GPC from **9** (290 mg, 0.5 mmol) and **1** (250 mg, 0.38 mmol), **11** (225 mg, 49%) was obtained as a green solid; m.p. >300 °C (decomp.); R_F = 0.10 (SiO_2, $CHCl_3$/MeOH, 95:5); UV–Vis (MeOH): λ_{max} (log ε) = 295 nm (4.27), 390 nm (4.29), 477 nm (397), 659 nm (4.63), 718 nm (5.01); IR (ATR): ν = 2925*w*, 1729*w*, 1624 *m*, 1577*w*, 1551*w*, 1441 *m*, 1400*w*, 1365 *m*, 1309*w*, 1268*w*, 1247*s*, 1227 *m*, 1167 *m*, 1143 *m*, 1097*s*, 1064*s*, 1043 *m*, 1018 *m*, 925 *m*, 860*w*, 811 *m*, 748 *m*, 670*w*, 622 m cm^{-1}; ^1H NMR (500 MHz, $CDCl_3$): δ = 8.57 (d, *J* = 13.4 Hz, 1H,

58-H), 7.58–7.48 (m, 2H, 40-H, 41-H), 7.46–7.32 (m, 3H, 42-H, 43-H, 62-H), 7.21 (*dd*, J = 28.5-H, 7.5 Hz, 3H, 53-H, 63-H, 65-H), 6.85–6.77 (m, 1H, 64-H), 6.70–6.46 (m, 2H, 55-H, 56-H), 6.14–5.99 (m, 1H, 59-H), 5.26–5.15 (m, 1H, 12-H), 4.50–4.44 (m, 1H, 3-H), 4.21–2.94 (m, 8H, 33-H, 34-H, 35-H, 37-H), 3.70 (d, J = 6.3 Hz, 3H, 68-H), 3.56–3.44 (m, 4H, 71-H, 73-H), 2.64 (s, 2H, 47-H), 2.42 (s, 1H, 16-H_b), 2.31 (s, 3H, 16-H_a, 49-H), 2.02 (s, 3H, 32-H), 2.15–1.69 (m, 5H, 11-H, 15-H_b, 48-H), 1.80–1.74 (m, 8H, 69-H, 70-H), 1.67–1.30 (m, 14H, 1-H_b, 2-H, 6-H, 7-H, 9-H, 18-H, 19-H, 21-H, 22-H), 1.26 (t, J = 6.5 Hz, 6H, 72-H, 74-H), 1.14–0.89 (m, 4H, 1-H_a, 5-H, 15-H_a, 20-H), 1.03 (s, 3H, 27-H), 0.93–0.88 (m, 9H, 23-H, 25-H, 29-H), 0.86–0.81 (m, 6H, 24-H, 30-H), 0.71 (s, 3H, 26-H) ppm; ^{13}C NMR (126 MHz, $CDCl_3$): δ = 176.6 (C-28), 174.1 (C-60), 171.1 (C-31), 168.6 (C-38), 163.1 (C-52), 155.7 (C-45), 152.2 (C-54), 152.1 (C-51), 143.0 (C-61), 142.9 (C-58), 140.8 (C-66), 140.7 (C-13), 135.5 (C-44), 132.7 (C-39), 129.9 (C-43), 129.8 (C-42), 129.2 (C-40), 129.1 (C-41), 128.9 (C-64), 127.0 (C-65), 125.6 (C-63), 125.1 (C-12), 122.9 (C-46), 122.4 (C-62), 116.1 (C-50), 113.3 (C-57), 111.9 (C-56), 110.9 (C-53), 99.7 (C-59), 96.1 (C-55), 81.0 (C-3), 55.4 (C-5), 49.4 (C-17), 49.0 (C-33), 49.0 (C-37), 47.9 (C-67), 47.8 (C-18), 47.7 (C-9), 46.6 (C-35), 46.5 (C-34), 45.3 (C-71, C-73), 42.2 (C-14), 39.8 (C-19), 38.8 (C-20), 38.3 (C-1), 37.8 (C-8), 37.0 (C-4, 10), 33.6 (C-22), 32.9 (C-7), 31.9 (C-68), 30.6 (C-21), 29.8 (C-36), 28.5 (C-69), 28.5 (C-70), 28.2 (C-15), 28.2 (C-23), 27.1 (C-16), 27.1 (C-49), 24.3 (C-47), 24.2 (C-27), 23.6 (C-2), 23.4 (C-11), 21.4 (C-29, 32), 20.6 (C-48), 18.3 (C-6), 17.6 (C-30), 17.1 (C-26), 16.8 (C-24), 15.6 (C-25), 12.6 (C-72, C-24) ppm; MS (ESI, MeOH/$CHCl_3$, 4:1): m/z (%) = 1122.4 (100%, $[M]^+$); anal. calcd for $C_{74}H_{97}N_4O_9Cl$ (1222.06), C 72.73, H 8.00, N 4.58; found: C 72.47, H 8.24, N 4.38.

4.8.12. 2α,3β-Bis(acetyloxy)urs-12-en-28-oic acid (12)

To a solution of banaba leaf extract powder (10.0 g, 20% corosolic acid, KAN Phytochemicals Pvt. Ltd) in pyridine (80 mL), acetic anhydride (20 mL) was added, and the reaction mixture was stirred at room temperature for 12–24 h (TLC). The solution was precipitated in aq. HCl (2 M). The solid was subjected to column chromatography (hexanes: ethyl acetate 15% → 40%), and compound **12** (1.95 g) was obtained as an off-white solid; R_f = 0.59 (*n*-hexane/ethyl acetate, 6:4); m. p. 235–238 °C (lit.: 237–241 °C [5]); $[\alpha]_D^{20}$ = +20.5° (*c* 0.25, $CHCl_3$) [lit.: $[\alpha]_D^{20}$ = +24.8° (*c* 0.15, $CHCl_3$) [5]]; MS (ESI, MeOH): m/z (%) = 625.5 (100%, $[M + H]^+$).

4.8.13. (2α, 3β) 2,3-Bis(acetyloxy)-28-(1-piperazinyl)-urs-12-en-28-one (13)

Following GPB from **12** (2.2 g, 4.0 mmol) and piperazine (1.36 g, 16.0 mmol), **13** (2.2 g, 88%) was obtained as a colorless solid; R_F = 0.14 (SiO_2, $CHCl_3$/MeOH, 95:5); m.p. 190–192 °C (lit.: 189–191 °C [5]); $[\alpha]_D^{20}$ = +8.3° (*c* 0.25, $CHCl_3$), (lit.: $[\alpha]_D^{20}$ = +10.3° (*c* 0.06, $CHCl_3$) [5,6]); MS (ESI, MeOH): m/z (%) = 639.4 (100%, $[M + H]^+$).

4.8.14. (2α, 3β) 2,3-Bis(acetyloxy)-28-(1-homopiperazinyl)-urs-12-en-28-one (14)

Following GPB from **12** (2.2 g, 4.0 mmol) and homopiperazine (1.6 g, 16.0 mmol), **14** (1.0 g, 78%) was obtained as a colorless solid; R_F = 0.13 (SiO_2, $CHCl_3$/MeOH, 95:5); m.p. 164–166 °C (lit.: 164–167 °C [5]); $[\alpha]_D^{20}$ = +12.7° (*c* 0.20, $CHCl_3$), (lit.: $[\alpha]_D^{20}$ = +9.0° (*c* 0.15, $CHCl_3$) [5]); MS (ESI, MeOH): m/z (%) = 639.2 (100%, $[M + H]^+$).

4.8.15. (E)-2-(2-[6-(diethylamino)-9-[2-[4-[(2α,3β)-bis(acetyloxy)-28-oxo-ursan-12-en-28-ylpiperazine-1-carbonyl]phenyl]-2,3-dihydro-1H-xanthen-4-yl]vinyl)-1,3,3-trimethyl-3H-indol-1-ium perchlorate (15)

Following GPC from **13** (312 mg, 0.5 mmol) and **1** (80 mg, 0.13 mmol), **15** (100 mg, 62%) was obtained as a green solid; m.p. >300 °C (decomp.); R_F = 0.10 (SiO_2, $CHCl_3$/MeOH, 95:5); UV–Vis (MeOH): λ_{max} (log ε) = 298 nm (4.10), 390 nm (4.14), 476 nm (3.80), 659 nm (4.40), 716 nm (4.76); IR (ATR): ν = 2927*w*, 1738 *m*, 1625 *m*, 1578*w*, 1552*w*, 1442 *m*, 1397*w*, 1366 *m*, 1310*w*, 1268*w*, 1248*s*, 1228 *m*, 1168 *m*, 1144 *m*, 1108*s*, 1067*s*, 1042 *m*, 1019 *m*, 927 *m*, 860*w*, 811 *m*, 749 *m*, 672*w*, 622 m cm^{-1}; ^{1}H NMR (500 MHz, $CDCl_3$): δ = 8.57 (d, J = 14.1 Hz, 1H, 59-H), 7.63–7.51 (m, 2H, 41-H, 44-H), 7.48–7.34 (m, 3H, 63-H, 65-H, 66-H), 7.25–7.15 (m, 3H, 42-H, 43-H, 64-H), 6.81 (s, 1H, 54-H), 6.68 (s, 1H, 57-H), 6.53 (s, 1H, 56-H), 6.09–6.03 (m, 1H, 60-H), 5.19 (t, J = 3.5 Hz, 1H, 12-H), 5.12–5.02 (m, 1H, 2-H), 4.72 (d, J = 10.3 Hz, 1H, 3-H), 3.69 (d, J = 5.7 Hz, 3H, 69-H), 3.64–3.54 (m, 4H, 35-H, 38-H), 3.50 (q, J = 7.0 Hz, 4H, 72-H, 74-H), 2.88–2.75 (m, 4H, 36-H, 37-H), 2.70–2.60 (m, 2H, 48-H), 2.45–2.25 (m, 5H, 16-H, 18-H, 50-H), 2.19–2.07 (m, 1H, 1-H_a), 2.03 (s, 3H, 34-H), 1.95 (s, 3H, 32-H), 2.01–1.80 (m, 4H, 11-H, 49-H), 1.77 (s, 6H, 70-H, 71-H), 1.72 (s, 3H, 15-H_b, 22-H), 1.60–1.27 (m, 8H, 6-H, 7-H, 9-H, 19-H, 21-H), 1.24 (t, J = 7.0 Hz, 6H, 73-H, 75-H), 1.12–0.97 (m, 4H, 1-H_b, 5-H, 15-H_a, 20-H), 1.04 (s, 3H, 25-H), 0.91 (d, J = 3.8 Hz, 3H, 29-H), 0.88 (s, 3H, 24-H), 0.88–0.87 (m, 6H, 23-H, 27-H), 0.84 (d, J = 6.4 Hz, 3H, 30-H), 0.74 (s, 3H, 26-H) ppm; ^{13}C NMR (126 MHz, $CDCl_3$): δ = 176.0 (C-28), 175.3 (C-61), 170.9 (C-31), 170.6 (C-33), 168.1 (C-39), 163.0 (C-53), 155.8 (C-46), 152.1 (C-52), 152.0 (C-55), 142.9 (C-62), 142.7 (C-59), 140.8 (C-13), 140.8 (C-67), 134.4 (C-45), 133.2 (C-40), 130.3 (C-44), 129.7 (C-43), 129.2 (C-41), 129.2 (C-42), 128.9 (C-65), 127.7 (C-66), 125.6 (C-64), 124.8 (C-12), 122.7 (C-47), 122.3 (C-63), 116.0 (C-51), 113.4 (C-58), 112.1 (C-57), 110.9 (C-54), 100.1 (C-60), 96.0 (C-56), 80.8 (C-3), 70.2 (C-2), 55.0 (C-5), 55.0 (C-18), 49.5 (C-17), 47.7 (C-9), 47.5 (C-35), 46.5 (C-38), 46.2 (C-36), 46.1 (C-68), 45.3 (C-72, C-24), 45.1 (C-37), 44.2 (C-1), 42.3 (C-14), 39.6 (C-19), 39.4 (C-8), 38.8 (C-20), 38.2 (C-4), 38.2 (C-10), 34.3 (C-22), 32.9 (C-7), 32.0 (C-69), 30.6 (C-21), 28.5 (C-23), 28.5 (C-70), 28.5 (C-71), 28.3 (C-15), 28.0 (C-50), 27.1 (C-16), 24.4 (C-48), 23.5 (C-11), 21.3 (C-32), 21.3 (C-27), 21.2 (C-34), 21.0 (C-29), 20.6 (C-49), 18.3 (C-6), 17.8 (C-24), 17.5 (C-30), 16.9 (C-26), 16.6 (C-25), 12.6 (C-73), 12.6 (C-75) ppm; MS (ESI, MeOH/$CHCl_3$, 4:1): m/z (%) = 1166.5 (100%, $[M]^+$); anal. calcd for $C_{75}H_{97}N_4O_{11}Cl$ (1266.07), C 71.15, H 7.72, N 4.43; found: C 70.92, H 7.93, N 4.18.

4.8.16. (E)-2-(2-[6-(diethylamino)-9-[2-[4-[(2α,3β)-bis(acetyloxy)-28-oxo-ursan-12-en-28-ylhomopiperazine-1-carbonyl]phenyl]-2,3-dihydro-1H-xanthen-4-yl]vinyl)-1,3,3-trimethyl-3H-indol-1-ium perchlorate (16)

Following GPC from **14** (319 mg, 0.5 mmol) and **1** (250 mg, 0.38 mmol), **16** (235 mg, 48%) was obtained as a green solid; m.p. >300 °C (decomp.); R_F = 0.10 (SiO_2, $CHCl_3$/MeOH, 95:5); UV–Vis (MeOH): λ_{max} (log ε) = 296 nm (4.36), 390 nm (4.41), 480 nm (4.11), 659 nm (4.58), 718 nm (5.01); IR (ATR): ν = 2928*w*, 1738*w*, 1624 *m*, 1577*w*, 1552*w*, 1441 *m*, 1399*w*, 1366 *m*, 1309*w*, 1268*w*, 1247*s*, 1226 *m*, 1167 *m*, 1143 *m*, 1099*s*, 1065*s*, 1042 *m*, 1018 *m*, 925 *m*, 860*w*, 811 *m*, 747 *m*, 669*w*, 622 m cm^{-1}; ^{1}H NMR (500 MHz, $CDCl_3$): δ = 8.56 (d, J = 13.0 Hz, 1H, 60-H), 7.58–7.48 (m, 2H, 42-H, 45-H), 7.45–7.31 (m, 3H, 43-H, 64-H, 67-H), 7.25–7.21 (m, 1H, 65-H), 7.20–7.15 (m, 2H, 44-H, 55-H), 6.85–6.75 (m, 1H, 66-H), 6.70–6.44 (m, 2H, 57-H, 58-H), 6.16–5.97 (m, 1H, 61-H), 5.23–5.15 (m, 1H, 12-H), 5.07 (*td*, J = 10.9Hz, 4.6 Hz, 1H, 2-H), 4.72 (d, J = 10.3 Hz, 1H, 3-H), 3.75–3.65 (m, 3H, 70-H), 3.51 (m, 4H, 73-H, 74-H), 4.32–2.82 (m, 8H, 35-H, 36-H, 37-H, 39-H), 2.77–2.53 (m, 3H, 16-H_b, 49-H), 2.53–2.20 (m, 4H, 16-H_a, 18-H, 51-H), 2.03 (s, 3H, 34-H), 1.95 (s, 3H, 32-H), 2.19–1.69 (m, 8H, 1-H_b, 11-H, 15-H_b, 38-H, 50-H), 1.80–1.74 (m, 6H, 71-H, 72-H), 1.68–1.15 (m, 10H, 6-H, 7-H, 9-H, 19-H, 21-H, 22-H), 1.29–1.22 (m, 6H, 75-H, 76-H), 1.12–0.81 (m, 4H, 1-H_a, 5-H, 15-H_a, 20-H), 1.08–1.03 (m, 3H, 30-H), 1.02 (s, 3H, 25-H), 0.96–0.91 (m, 3H, 29-H), 0.88–0.86 (m, 9H, 23-H, 24-H, 27-H), 0.71 (s, 3H, 26-H) ppm; ^{13}C NMR (126 MHz, $CDCl_3$): δ = 176.6 (C-28), 174.1 (C-62), 170.9 (C-31), 170.6 (C-33), 168.5 (C-40), 163.1 (C-54), 155.8 (C-47), 152.2 (C-53), 152.1 (C-56), 142.9 (C-63), 142.9 (C-60), 140.8 (C-68), 140.7 (C-13), 135.4 (C-46), 132.7 (C-41), 129.9 (C-45), 129.8 (C-44), 129.1 (C-42), 129.0 (C-43), 128.9 (C-66), 126.9 (C-67), 125.5 (C-65), 124.7 (C-12), 124.0 (C-48), 122.4 (C-64), 116.1 (C-52), 113.4 (C-59), 112.0 (C-58), 110.9 (C-55), 100.7 (C-61), 95.7 (C-57), 80.7 (C-3), 70.2 (C-2), 55.0 (C-5, 18), 49.5 (C-39), 49.4 (C-17), 48.9 (C-37), 47.8 (C-35), 47.6 (C-9), 46.7 (C-36), 45.3 (C-73, 74), 45.2 (C-69), 44.2 (C-1),

42.7 (C-14), 39.4 (C-8), 39.3 (C-19), 38.7 (C-20), 38.2 (C-4, 10), 33.7 (C-22), 32.9 (C-7), 31.9 (C-70), 30.6 (C-21), 29.8 (C-38), 28.5 (C-71, C-72), 28.5 (C-23), 28.0 (C-15), 27.9 (C-51), 27.1 (C-16), 24.3 (C-49), 23.4 (C-11), 21.4 (C-32), 21.3 (C-34), 21.2 (C-27), 21.0 (C-29), 20.6 (C-50), 18.2 (C-6), 17.7 (C-24), 17.5 (C-26), 16.9 (C-30), 16.6 (C-25), 12.6 (C-75), 12.6 (C-76) ppm; MS (ESI, MeOH/$CHCl_3$, 4:1): *m/z* (%) = 1180.3 (100%, $[M]^+$); anal. calcd for $C_{76}H_{99}N_4O_{11}Cl$ (1280.10), C 71.31, H 7.80, N 4.38; found: C 71.04, H 7.99, N 4.17.

4.8.17. 2α,3β,23-Tris(acetyloxy)-urs-12-en-28-oic acid (17)

Following GPA, compound **7** (1.85 g, 89%) was obtained from **AA** (1.65 g, 3.5 mmol) as a colorless solid; $R_F = 0.33$ (*n*-hexane/ethyl acetate, 7:3); m.p. 161–162 °C (lit.: 159–161 °C [10]); $[\alpha]_D^{20} = +33.8°$ (*c* 0.20, $CHCl_3$) (lit.: $[\alpha]_D^{20} = +35.9°$ (*c* 0.34, $CHCl_3$) [10]); MS (ESI, MeOH): *m/z* (%) = 615.3 (100%, $[M + H]^+$).

4.8.18. 2α,3β,23-Tris(acetyloxy)-28-(1-piperazinyl)-urs-12-en-28-one (18)

Following GPB from **17** (2.4 g, 4.0 mmol) and piperazine (1.36 g, 16.0 mmol), **19** (2.4 g, 89%) was obtained as a colorless solid; $R_F = 0.12$ (SiO_2, $CHCl_3$/MeOH, 95:5); m.p. 156–159 °C (lit.: 157–160 °C [10]); $[\alpha]_D^{20} = +20.1°$ (*c* 0.25, $CHCl_3$), (lit.: $[\alpha]_D^{20} = +17.7°$ (*c* 0.27, $CHCl_3$) [10]); MS (ESI, MeOH): *m/z* (%) = 683.2 (100%, $[M + H]^+$).

4.8.19. 2α,3β,23-Tris(acetyloxy)-28-(1-homopiperazinyl)-urs-12-en-28-one (19)

Following GPB from **17** (2.2 g, 4.0 mmol) and homopiperazine (1.6 g, 16.0 mmol), **19** (2.51 g, 91%) was obtained as a colorless solid; $R_F = 0.15$ (SiO_2, $CHCl_3$/MeOH, 95:5); m.p. 185–186 °C (lit.: 185–186 °C [12]); $[\alpha]_D^{20} = +15.9°$ (*c* 0.15, $CHCl_3$), (lit.: $[\alpha]_D^{20} = +14.4°$ (*c* 0.14, $CHCl_3$) [12]); MS (ESI, MeOH): *m/z* (%) = 683.0 (100%, $[M + H]^+$).

4.8.20. (E)-2-(2-[6-(diethylamino)-9-[2-[4-[(2α,3β, 23)-tris(acetyloxy)-28-oxo-ursan-12-en-28-ylpiperazine-1-carbonyl]phenyl]-2,3-dihydro-1H-xanthen-4-yl]vinyl)-1,3,3-trimethyl-3H-indol-1-ium perchlorate (20)

Following GPC from **18** (334 mg, 0.5 mmol) and **1** (125 mg, 0.19 mmol), **20** (125 mg, 50%) was obtained as a green solid; m.p. >300 °C (decomp.); $R_F = 0.10$ (SiO_2, $CHCl_3$/MeOH, 95:5); UV–Vis (MeOH): λ_{max} (log ε) = 295 nm (4.22), 390 nm (4.34), 475 nm (4.04), 658 nm (4.52), 716 nm (4.89); IR (ATR): ν = 2926*w*, 1739*w*, 1624 *m*, 1577*w*, 1551*w*, 1440 *m*, 1399*w*, 1365 *m*, 1309*w*, 1268*w*, 1247*s*, 1226 *m*, 1154 *m*, 1143 *m*, 1095*s*, 1065*s*, 1042*s*, 1004 *m*, 925 *m*, 860*w*, 811 *m*, 749 *m*, 672*w*, 622 m cm^{-1}; ^1H NMR (500 MHz, $CDCl_3$): δ = 8.57 (d, *J* = 14.1 Hz, 1H, 59-H), 7.62–7.52 (m, 2H, 41-H, 44-H), 7.41 (*dt*, *J* = 17.8 Hz, 8.7 Hz, 3H, 43-H, 63-H, 66-H), 7.27–7.17 (m, 3H, 42-H, 54-H, 64-H), 6.82 (t, *J* = 11.6 Hz, 1H, 65-H), 6.77–6.67 (m, 1H, 57-H), 6.53 (s, 1H, 56-H), 6.06 (d, *J* = 13.9 Hz, 1H, 60-H), 5.17 (s, 1H, 12-H), 5.13 (*td*, *J* = 11.0-H, 4.5 Hz, 1H, 2-H), 5.06 (dd, *J* = 10.3 Hz, 1.8 Hz, 1H, 3-H), 3.88–3.78 (m, 1H, 23-H_b), 3.70 (d, *J* = 5.1 Hz, 3H, 69-H), 3.56 (dd, *J* = 11.8 Hz, 7.9 Hz, 1H, 23-H_a), 3.50 (q, *J* = 6.9 Hz, 4H, 72-H, 74-H), 3.32 (s, 8H, 37-H, 38-H), 2.65 (s, 2H, 48-H), 2.52 (s, 1H, 16-H_b), 2.33 (s, 2H, 16-H_a, 18-H), 2.07 (s, 3H, 36-H), 2.00 (s, 3H, 34-H), 1.96 (s, 3H, 32-H), 1.90 (s, 4H, 1-H_a, 11-H, 15-H_b), 1.82 (s, 3H, 22-H_a, 49-H), 1.77 (s, 6H, 70-H, 71-H), 1.59 (d, *J* = 9.2 Hz, 1H, 9-H), 1.51–1.28 (m, 11H, 5-H, 6-H, 7-H, 19-H, 21-H, 22-H_b, 50-H), 1.25 (t, *J* = 7.0 Hz, 6H, 73-H, 75-H), 1.16–0.92 (m, 3H, 1-H_b, 15-H_a, 20-H), 1.06 (s, 3H, 25-H), 1.04 (s, 3H, 27-H), 0.91 (d, *J* = 5.9 Hz, 3H, 29-H), 0.86 (s, 3H, 24-H), 0.83 (d, *J* = 6.0 Hz, 3H, 30-H), 0.68 (s, 3H, 26-H) ppm; ^{13}C NMR (126 MHz, $CDCl_3$): δ = 176.0 (C-28), 174.0 (C-61), 171.0 (C-35), 170.5 (C-33), 170.4 (C-31), 168.2 (C-39), 163.0 (C-53), 155.8 (C-46), 152.1 (C-52), 152.1 (C-55), 142.9 (C-62), 142.7 (C-59), 140.8 (C-67), 140.8 (C-13), 134.4 (C-45), 133.2 (C-40), 130.3 (C-44), 130.3 (C-43), 129.7 (C-41), 129.3 (C-42), 128.9 (C-65), 127.6 (C-66), 125.6 (C-64), 124.8 (C-12), 122.6 (C-47), 122.3 (C-63), 116.0 (C-51), 113.5 (C-58), 112.2 (C-57), 111.0 (C-54), 100.0 (C-60), 96.1 (C-56), 75.0 (C-3), 70.0 (C-2), 55.8 (C-18), 49.5 (C-17), 48.7 (C-37), 47.7 (C-5), 47.6 (C-9), 47.5 (C-38), 46.3 (C-68), 45.3 (C-72, C-24), 43.8 (C-1), 42.0 (C-14), 39.5 (C-8), 39.4 (C-19), 38.8 (C-20), 37.9 (C-4, 10), 34.3 (C-22), 32.6 (C-7), 32.0 (C-69), 30.5 (C-21), 28.5 (C-70), 28.5 (C-71), 28.1 (C-15), 28.1 (C-50), 27.1 (C-16), 24.4 (C-48), 23.4 (C-11), 21.3 (C-27, 29), 21.2 (C-36), 21.0 (C-32), 20.9 (C-34), 20.6 (C-49), 18.0 (C-6), 17.4 (C-25), 17.1 (C-26), 17.1 (C-30), 14.0 (C-24), 12.6 (C-73, 75) ppm; MS (ESI, MeOH/$CHCl_3$, 4:1): *m/z* (%) = 1224.0 (100%, $[M]^+$); anal. calcd for $C_{77}H_{99}N_4O_{13}Cl$ (1324.10), C 69.85, H 7.54, N 4.23; found: C 69.67, H 7.81, N 4.02.

4.8.21. (E)-2-(2-[6-(diethylamino)-9-[2-[4-[(2α,3β,23)-tris(acetyloxy)-28-oxo-ursan-12-en-28-ylhomopiperazine-1-carbonyl]phenyl]-2,3-dihydro-1H-xanthen-4-yl]vinyl)-1,3,3-trimethyl-3H-indol-1-ium perchlorate (21)

Following GPC from **19** (341 mg, 0.5 mmol) and **1** (250 mg, 0.38 mmol), **21** (335 mg, 66%) was obtained as a green solid; m.p. >300 °C (decomp.); $R_F = 0.10$ (SiO_2, $CHCl_3$/MeOH, 95:5); UV–Vis (MeOH): λ_{max} (log ε) = 297 nm (4.28), 390 nm (4.32), 477 nm (3.98), 660 nm (4.68), 719 nm (5.06); IR (ATR): ν = 2926*w*, 1739*w*, 1624 *m*, 1577*w*, 1551*w*, 1441 *m*, 1366*w*, 1309*w*, 1268*w*, 1248*s*, 1225 *m*, 1167 *m*, 1143 *m*, 1103*s*, 1064*s*, 1042 *m*, 1018 *m*, 925 *m*, 860*w*, 811 *m*, 747 *m*, 668*w*, 622 m cm^{-1}; ^1H NMR (500 MHz, $CDCl_3$): δ = 8.60–8.52 (m, 1H, 62-H), 7.59–7.48 (m, 2H, 46-H, 47-H), 7.44–7.30 (m, 4H, 44-H, 45-H, 66-H, 70-H), 7.25–7.22 (m, 1H, 67-H), 7.21–7.16 (m, 1H, 57-H), 6.89–6.75 (m, 1H, 68-H), 6.69–6.46 (m, 2H, 59-H, 60-H), 6.16–5.97 (m, 1H, 63-H), 5.20–5.18 (m, 1H, 12-H), 5.14 (*td*, *J* = 11.0 Hz, 4.6 Hz, 1H, 2-H), 5.05 (d, *J* = 10.3 Hz, 1H, 3-H), 3.82 (d, *J* = 11.6 Hz, 1H, 23-H_b), 3.69 (d, *J* = 6.0 Hz, 3H, 69-H), 3.56 (d, *J* = 12.0 Hz, 1H, 23-H_a), 3.54–3.43 (m, 4H, 75-H, 76-H), 4.21–2.98 (m, 8H, 37-H, 38-H, 39-H, 41-H), 2.75–2.53 (m, 2H, 51-H), 2.51–2.38 (m, 1H, 16-H_b), 2.36–2.20 (m, 2H, 16-H_a, 18-H), 2.06 (s, 3H, 36-H), 2.00 (s, 3H, 34-H), 1.95 (s, 3H, 32-H), 2.15–1.69 (m, 6H, 1-H_a, 11-H, 15-H_a, 52-H), 1.77 (d, *J* = 4.8 Hz, 6H, 73-H, 74-H), 1.67–1.53 (m, 5H, 9-H, 40-H, 53-H), 1.53–1.18 (m, 10H, 5-H, 6-H, 7-H, 19-H, 21-H, 22-H), 1.26 (t, *J* = 6.6 Hz, 6H, 77-H, 78-H), 1.06 (s, 3H, 27-H), 1.16–0.88 (m, 3H, 1-H_b, 15-H_b, 20-H), 1.04 (d, *J* = 8.8 Hz, 3H, 30-H), 0.90 (d, *J* = 6.0 Hz, 3H, 29-H), 0.86 (s, 6H, 24-H, 25-H), 0.72 (s, 3H, 26-H) ppm; ^{13}C NMR (126 MHz, $CDCl_3$): δ = 173.8 (C-28), 170.9 (C-35), 170.5 (C-31), 170.4 (C-33), 169.1 (C-64), 168.6 (C-42), 163.1 (C-56), 155.7 (C-49), 152.2 (C-58), 152.1 (C-55), 142.9 (C-65), 142.6 (C-62), 140.8 (C-71), 140.8 (C-13), 135.4 (C-48), 132.7 (C-43), 129.9 (C-47), 129.8 (C-46), 129.2 (C-44), 129.1 (C-45), 128.9 (C-68), 126.9 (C-70), 125.5, 124.6 (C-12, 67), 123.3 (C-50), 122.3 (C-66), 116.1 (C-54), 113.4 (C-61), 112.0 (C-60), 110.9 (C-57), 99.6 (C-63), 95.8 (C-59), 75.0 (C-3), 70.0 (C-2), 65.4 (C-23), 55.2 (C-18), 49.4 (C-17), 49.0 (C-41), 48.2 (C-37), 48.1 (C-39), 47.8 (C-38), 47.8 (C-9), 47.7 (C-5), 46.4 (C-72), 45.3 (C-75, 76), 43.8 (C-1), 42.0 (C-14), 39.4 (C-8), 38.9 (C-19), 38.7 (C-20), 37.9 (C-4, 10), 33.8 (C-22), 32.7 (C-7), 31.9 (C-69), 30.6 (C-21), 29.7 (C-40), 28.5 (C-73), 28.5 (C-74), 28.0 (C-53), 28.0 (C-15), 27.1 (C-16), 24.3 (C-51), 23.4 (C-11), 21.4 (C-27), 21.3 (C-29), 21.2 (C-36), 21.0 (C-34), 20.9 (C-32), 20.6 (C-52), 18.0 (C-6), 17.5 (C-26), 17.5 (C-25), 17.1 (C-30), 14.0 (C-24), 12.6 (C-78), 12.6 (C-77) ppm; MS (ESI, MeOH/$CHCl_3$, 4:1): *m/z* (%) = 1238.2 (100%, $[M]^+$); anal. calcd for $C_{78}H_{101}N_4O_{13}Cl$ (1338.13), C 70.01, H 7.61, N 4.19; found: C 69.82, H 7.80, N 3.97.

Declaration of competing interest

The authors declare that they have no known competing financial interests or personal relationships that could have appeared to influence the work reported in this paper.

Data availability

No data was used for the research described in the article.

Acknowledgments

We like to thank Th. Schmidt for numerous MS spectra as well as Dr.

D. Ströhl, Y. Schiller and S. Ludwig for additional NMR spectra. UV/Vis and IR spectra were recorded by M. Schneider who also performed the micro-analyses.

Appendix A. Supplementary data

Supplementary data to this article can be found online at https://doi.org/10.1016/j.ejmech.2023.115663.

References

[1] H. Sung, J. Ferlay, R.L. Siegel, M. Laversanne, I. Soerjomataram, A. Jemal, F. Bray, Global cancer statistics 2020: GLOBOCAN estimates of incidence and mortality worldwide for 36 cancers in 185 countries, CA, Cancer J. Clin. 71 (2021) 209–249.
[2] P. Palekar-Shanbhag, S.V. Jog, M.M. Chogale, S.S. Gaikwad, Theranostics for cancer therapy, Curr. Drug Deliv. 10 (2013) 357–362.
[3] S. Jeelani, R.C.J. Reddy, T. Maheswaran, G.S. Asokan, A. Dany, B. Anand, Theranostics: a treasured tailor for tomorrow, J. Pharm. BioAllied Sci. 6 (2014) S6–S8.
[4] R.K. Wolfram, L. Heller, R. Csuk, Targeting mitochondria: esters of rhodamine B with triterpenoids are mitocanic triggers of apoptosis, Eur. J. Med. Chem. 152 (2018) 21–30.
[5] N.V. Heise, S. Hoenke, I. Serbian, R. Csuk, An improved partial synthesis of corosolic acid and its conversion to highly cytotoxic mitocans, Eur. J. Med. Chem. Rep. 6 (2022), 100073.
[6] N.V. Heise, D. Major, S. Hoenke, M. Kozubek, I. Serbian, R. Csuk, Rhodamine 101 conjugates of triterpenoic amides are of comparable cytotoxicity as their rhodamine B analogs, Molecules 27 (2022) 2220.
[7] N. Heise, S. Hoenke, V. Simon, H.-P. Deigner, A. Al-Harrasi, R. Csuk, Type and position of linkage govern the cytotoxicity of oleanolic acid rhodamine B hybrids, Steroids 172 (2021), 108876.
[8] S. Hoenke, N.V. Heise, M. Kahnt, H.-P. Deigner, R. Csuk, Betulinic acid derived amides are highly cytotoxic, apoptotic and selective, Eur. J. Med. Chem. 207 (2020), 112815.
[9] M. Kahnt, L. Fischer, A. Al-Harrasi, R. Csuk, Ethylenediamine derived carboxamides of betulinic and ursolic acid as potential cytotoxic agents, Molecules 23 (2018) 2558.
[10] M. Kahnt, J. Wiemann, L. Fischer, S. Sommerwerk, R. Csuk, Transformation of asiatic acid into a mitocanic, bimodal-acting rhodamine B conjugate of nanomolar cytotoxicity, Eur. J. Med. Chem. 159 (2018) 143–148.
[11] R.K. Wolfram, L. Fischer, R. Kluge, D. Ströhl, A. Al-Harrasi, R. Csuk, Homopiperazine-rhodamine B adducts of triterpenoic acids are strong mitocans, Eur. J. Med. Chem. 155 (2018) 869–879.
[12] O. Kraft, A.-K. Hartmann, S. Brandt, S. Hoenke, N.V. Heise, R. Csuk, T. Mueller, Asiatic acid as a leading structure for derivatives combining sub-nanomolar cytotoxicity, high selectivity, and the ability to overcome drug resistance in human preclinical tumor models, Eur. J. Med. Chem. 250 (2023), 115189.
[13] R. Borlan, M. Focsan, D. Maniu, S. Astilean, Interventional NIR fluorescence imaging of cancer: review on next generation of dye-loaded protein-based nanoparticles for real-time feedback during cancer surgery, Int. J. Nanomed. 16 (2021) 2147–2171.
[14] L.K.A. Neijenhuis, L.D.A.N. de Myunck, O.D. Bijlstra, P.J.K. Kuppen, D.E. Hilling, F. J. Borm, D. Cohen, J.S.D. Mieog, W.H. Steup, J. Braun, J. Burggraaf, A. L. Vahrmeijer, M. Hutteman, Near-infrared fluorescence tumor-targeted imaging in lung cancer: a systematic review, Life 12 (2022) 446.
[15] J. Rao, A. Dragulescu-Andrasi, H. Yao, Fluorescence imaging in vivo: recent advances, Curr. Opin. Biotechnol. 18 (2007) 17–25.
[16] S.A. Hilderbrand, R. Weissleder, Near-infrared fluorescence: application to in vivo molecular imaging, Curr. Opin. Chem. Biol. 14 (2010) 71–79.
[17] D.D. Nolting, J.C. Gore, W. Pham, Near-infrared dyes: probe development and applications in optical molecular imaging, Curr. Org. Synth. 8 (2011) 521–534.
[18] Z. Guo, S. Park, J. Yoon, I. Shin, Recent progress in the development of near-infrared fluorescent probes for bioimaging applications, Chem. Soc. Rev. 43 (2014) 16–29.
[19] R.F. Kubin, A.N. Fletcher, Fluorescence quantum yields of some rhodamine dyes, J. Lumin. 27 (1982) 455–462.
[20] L. Yuan, W. Lin, Y. Yang, H. Chen, A unique class of near-infrared functional fluorescent dyes with carboxylic-acid-modulated fluorescence ON/OFF switching: rational design, synthesis, optical properties, theoretical calculations, and applications for fluorescence imaging in living animals, J. Am. Chem. Soc. 134 (2012) 1200–1211.
[21] K. Karaoglu, K. Kaya, I. Yilmaz, New Chromenylium−cyanine based dual channel chemosensors for copper and hypochlorite sensing, Dyes Pigments 180 (2020), 108445.
[22] G.K. Vegesna, J. Janjanam, J. Bi, F.-T. Luo, J. Zhang, C. Olds, A. Tiwari, H. Liu, pH-activatable near-infrared fluorescent probes for detection of lysosomal pH inside living cells, J. Mater. Chem. B 2 (2014) 4500–4508.
[23] J.-Y. Xie, C.-Y. Li, Y.-F. Li, J. Fei, F. Xu, J. Ou-Yang, J. Liu, Near-infrared fluorescent probe with high quantum yield and its application in the selective detection of glutathione in living cells and tissues, Anal. Chem. 88 (2016) 9746–9752.
[24] L. Tong, Y. Qian, A NIR rhodamine fluorescent chemodosimeter specific for glutathione: knoevenagel condensation, detection of intracellular glutathione and living cell imaging, J. Mater. Chem. B 6 (2018) 1791–1798.
[25] X. Yang, Y. Qian, A NIR facile, cell-compatible fluorescent sensor for glutathione based on Michael addition induced cascade spirolactam opening and its application in hepatocellular carcinoma, J. Mater. Chem. B 6 (2018) 7486–7494.
[26] J.-Y. Xie, C.-Y. Li, Y.-F. Li, Y.-J. Fu, S.-X. Nie, H.-Y. Tan, A near-infrared chemosensor for determination of trivalent aluminum ions in living cells and tissues, Dyes Pigments 136 (2017) 817–824.
[27] K. Karaoglu, A new chromenylium-cyanine chemosensor for switch-ON near-infrared copper (II) sensing, J. Mol. Struct. 1205 (2020), 127640.
[28] D. Cheng, J. Peng, Y. Lv, D. Su, D. Liu, M. Chen, L. Yuan, X. Zhang, De novo design of chemical stability near-infrared molecular probes for high-fidelity hepatotoxicity evaluation in vivo, J. Am. Chem. Soc. 141 (2019) 6352–6361.
[29] H. Singh, J.Y. Lim, A. Sharma, D.W. Yoon, J.H. Kim, Z. Yang, J. Qu, J. Kim, S. G. Lee, J.S. Kim, A pH-responsive glycyrrhetinic-acid-modified small-molecule conjugate for NIR imaging of hepatocellular carcinoma (HCC), Chembiochem 20 (2019) 614–620.
[30] A.-K. Heinrich, H. Lucas, L. Schindler, P. Chytil, T. Etrych, K. Mäder, T. Mueller, Improved tumor-specific drug accumulation by polymer therapeutics with pH-sensitive drug release overcomes chemotherapy resistance, Mol. Cancer Therapeut. 15 (2016) 998–1007.